Article

Molecular Cell

CRISPR RNA-Dependent Binding and Cleavage of Endogenous RNAs by the *Campylobacter jejuni* Cas9

Graphical Abstract

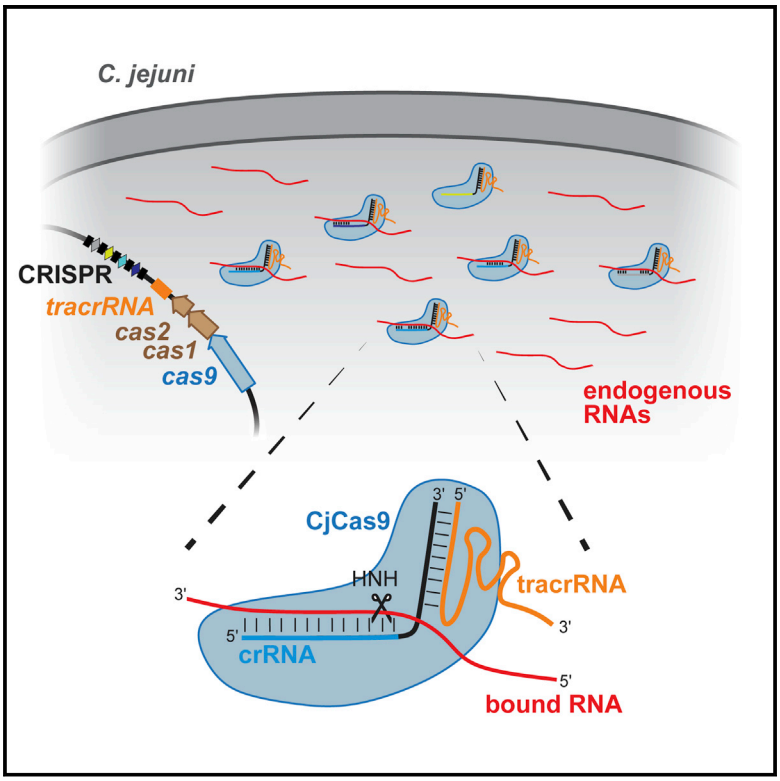

Highlights

- RIP-seq of the *Campylobacter jejuni* (Cj)Cas9 revealed numerous bound cellular RNAs
- Most RNAs were co-purified with the CjCas9 in a crRNA-dependent manner
- Some of the co-purified RNAs underwent cleavage dependent on the CjCas9 HNH domain
- RNA cleavage by CjCas9 was programmable by an sgRNA *in vitro*

Authors

Gaurav Dugar, Ryan T. Leenay, Sara K. Eisenbart, Thorsten Bischler, Belinda U. Aul, Chase L. Beisel, Cynthia M. Sharma

Correspondence

cbeisel@ncsu.edu (C.L.B.), cynthia.sharma@uni-wuerzburg.de (C.M.S.)

In Brief

CRISPR-Cas9 nucleases typically target double-stranded DNA targets. Dugar et al. show that one of the smallest Cas9 proteins (from *Campylobacter jejuni*) can also target endogenous RNAs. Targeting occurred through imperfect complementarity with native crRNA guides and cleavage by Cas9's HNH domain.

Dugar et al., 2018, Molecular Cell *69*, 893–905
March 1, 2018 © 2018 Elsevier Inc.
https://doi.org/10.1016/j.molcel.2018.01.032

CellPress

Molecular Cell
Article

CRISPR RNA-Dependent Binding and Cleavage of Endogenous RNAs by the *Campylobacter jejuni* Cas9

Gaurav Dugar,[1] Ryan T. Leenay,[2,4] Sara K. Eisenbart,[1,4] Thorsten Bischler,[1,4] Belinda U. Aul,[1] Chase L. Beisel,[2,3,*] and Cynthia M. Sharma[1,5,*]

[1]Institute of Molecular Infection Biology (IMIB)/Research Center for Infectious Diseases (ZINF), University of Würzburg, Josef-Schneider-Str. 2 / D15, D-97080 Würzburg, Germany
[2]Department of Chemical and Biomolecular Engineering, North Carolina State University, Raleigh, NC 27695, USA
[3]Helmholtz Institute for RNA-based Infection Research (HIRI), Josef-Schneider-Str. 2 / D15, D-97080 Würzburg, Germany
[4]These authors contributed equally
[5]Lead Contact
*Correspondence: cbeisel@ncsu.edu (C.L.B.), cynthia.sharma@uni-wuerzburg.de (C.M.S.)
https://doi.org/10.1016/j.molcel.2018.01.032

SUMMARY

Cas9 nucleases naturally utilize CRISPR RNAs (crRNAs) to silence foreign double-stranded DNA. While recent work has shown that some Cas9 nucleases can also target RNA, RNA recognition has required nuclease modifications or accessory factors. Here, we show that the *Campylobacter jejuni* Cas9 (CjCas9) can bind and cleave complementary endogenous mRNAs in a crRNA-dependent manner. Approximately 100 transcripts co-immunoprecipitated with CjCas9 and generally can be subdivided through their base-pairing potential to the four crRNAs. A subset of these RNAs was cleaved around or within the predicted binding site. Mutational analyses revealed that RNA binding was crRNA and tracrRNA dependent and that target RNA cleavage required the CjCas9 HNH domain. We further observed that RNA cleavage was PAM independent, improved with greater complementarity between the crRNA and the RNA target, and was programmable *in vitro*. These findings suggest that *C. jejuni* Cas9 is a promiscuous nuclease that can coordinately target both DNA and RNA.

INTRODUCTION

Clustered regularly interspaced short palindromic repeats (CRISPR) and their associated CRISPR-associated (Cas) proteins form adaptive immune systems in prokaryotes that rely on RNA-guided nucleases to target foreign genetic material (Koonin et al., 2017; Makarova et al., 2015; Mohanraju et al., 2016). The guide RNAs are encoded within repeat-spacer arrays that are transcribed and processed into individual CRISPR RNAs (crRNAs) that complex with Cas nucleases. The resulting ribonucleoprotein effector complex surveils the prokaryotic cytoplasm and cleaves invading nucleic-acid targets that are complementary to the crRNA guide and flanked by a protospacer-adjacent motif (PAM) or a protospacer-flanking sequence (PFS) (Leenay and Beisel, 2017). The addition of new spacers to the arrays from the invading viral or plasmid nucleic acids grants the adaptive component to CRISPR-Cas systems (Marraffini, 2015).

Despite a common role in host defense, CRISPR-Cas systems are remarkably diverse. The current classification scheme comprises 2 classes (class 1: multi-protein effector complexes; class 2: single protein effectors), 6 types, and at least 29 subtypes (Koonin et al., 2017; Makarova et al., 2015). While most CRISPR-Cas systems target double-stranded DNA (dsDNA), some systems target both DNA and RNA (Type III Cmr complexes) or only RNA (Type VI, C2c2/Cas13a) (Mohanraju et al., 2016). The diversity of these CRISPR systems has been exploited for various biotechnological applications, with the Type II Cas9 as the most prominently used nuclease (Jiang and Doudna, 2017). Type II systems are widespread in bacterial pathogens and commensals, and their crRNAs are processed through base pairing with a *trans*-activating CRISPR RNA (tracrRNA) encoded next to the CRISPR array and cleaved by RNase III (Deltcheva et al., 2011). The processed crRNA:tracrRNA duplex then complexes with Cas9 to bind and cleave double-stranded DNA complementary to the crRNA guide, flanked by a 3′ PAM (Gasiunas et al., 2012; Jinek et al., 2012).

While Cas9 is traditionally viewed as a DNA-targeting nuclease, emerging examples have highlighted the ability of Cas9 to target RNA. For instance, the *Francisella novicida* Cas9 native to its Type II-B CRISPR-Cas system downregulates the expression of an immunostimulatory bacterial lipoprotein (BLP) through tracrRNA in association with a small CRISPR-Cas-associated RNA (scaRNA) and thereby affects virulence as well as envelope integrity-mediated antibiotic resistance (Sampson et al., 2013, 2014). The exact mechanism of *blp* downregulation remains unclear but appears to be through base pairing between the scaRNA, tracrRNA, and the *blp* mRNA. Separately, the Type II-A Cas9 from *Streptococcus pyogenes* was shown to bind and cleave RNA paired *in vitro* to a PAM-encoding DNA oligonucleotide (PAMmer) (O'Connell et al., 2014). This capability of RNA-targeting Cas9 (RCas9) allowed for programmable RNA imaging with a catalytically dead variant of

Cas9 (Nelles et al., 2016). Recently, RCas9 fused to a PIN RNA endonuclease domain was employed to target disease-associated microsatellite expansion repeat RNAs (Batra et al., 2017). Interestingly, here the PAMmer was dispensable, although it is unclear whether this dispensability is due to the repetitive and semi-palindromic nature of the targeted microsatellite sequences. Despite these accumulating examples of Cas9 targeting RNA, it remains to be seen whether any Cas9 can naturally target RNA through its associated crRNAs.

Here, we show that the Type II-C Cas9 native to the foodborne bacterial pathogen *Campylobacter jejuni* (CjCas9) can bind and cleave endogenous RNAs through interaction with native crRNAs. RNA co-immunoprecipitation and sequencing revealed multiple endogenous RNAs that were enriched upon co-immunoprecipitation of CjCas9 in addition to tracrRNA and crRNAs. The majority appeared to base pair with the guide portion of one of the four encoded crRNAs. A fraction of the RNAs underwent cleavage in the vicinity of the predicted crRNA binding site. Further analysis of one representative target revealed that RNA cleavage required the HNH domain of CjCas9, was independent of a PAM, and could be reprogrammed using synthetic single-guide RNAs (sgRNAs). In total, these results indicate that CjCas9 has the natural ability to target endogenous RNAs through crRNAs and tracrRNA. Given the promise of CjCas9 as the smallest Cas9 available to date for CRISPR technologies (Kim et al., 2017; Yamada et al., 2017), these findings could enable CRISPR-based applications in coordinated DNA and RNA targeting.

RESULTS

RIP-Seq Identifies RNAs that Co-immunoprecipitate with CjCas9 in *C. jejuni*

Our global transcriptome analysis of multiple *C. jejuni* strains revealed the crRNAs and tracrRNA of the Type II-C CRISPR-Cas system as some of the most abundantly transcribed RNAs of *C. jejuni* strain NCTC11168 (Dugar et al., 2013). To study the potential capacity for RNA targeting by CjCas9, we employed a co-immunoprecipitation (coIP) approach combined with RNA-sequencing (RIP-seq) (Rieder et al., 2012; Sittka et al., 2008). The *cas9* gene (*cj1523c*) was chromosomally 3xFLAG-tagged at its C terminus in *C. jejuni* strain NCTC11168. We performed a coIP on the *cas9*-3xFLAG strain and, as a control, the untagged wild-type (WT) strain. Western blot analysis confirmed successful coIP of CjCas9 in the tagged strain (Figure 1A). *C. jejuni* NCTC11168 harbors a Type II-C CRISPR locus with four spacers (S1–S4, Figure 1B). While most crRNAs described in other bacteria are transcribed as a precursor and then processed into the mature crRNAs, each repeat within the CRISPR locus in *C. jejuni* and *Neisseria meningitidis* harbors a −10 promoter box to drive the transcription of downstream crRNAs and also the tracrRNA (Dugar et al., 2013; Zhang et al., 2013) (Figure 1B). After conversion of CjCas9 co-purified RNAs into cDNA and deep sequencing, reads for the libraries were mapped to the NCTC11168 genome (Table S1). Most of the control coIP library reads mapped to presumably non-specifically pulled-down abundant classes of RNA (rRNA, tRNA, and housekeeping RNAs) (Figure S1A; Table S1). In contrast, the Cas9 coIP library revealed strong enrichment of the tracrRNA and all four crRNAs when compared with the control library (Figures 1B and S1A; Table S1), indicating successful coIP of Cas9-crRNA-tracrRNA complexes.

Surprisingly, we noticed that many other RNAs aside from the tracrRNA and crRNAs were enriched in the Cas9 coIP versus the control coIP. To automatically and precisely identify enriched RNAs globally, we employed our previously developed peak-detection algorithm based on a sliding-window approach (Dugar et al., 2016). This approach identified 112 distinct RNA peaks with >5-fold enrichment in the Cas9 coIP library compared to the control library. The 112 peaks were then manually refined (see STAR Methods), resulting in 96 enriched peaks with an average length of 177 nts (Figure 1C; Table S2). The peaks were mainly found within the coding region of mRNAs, although others fell within antisense RNAs, tRNAs, and the untranslated regions of mRNAs (Figure 1C). These results suggest that Cas9 can directly or indirectly bind these RNAs, resulting in their co-immunoprecipitation.

crRNA-Dependent Binding of Endogenous RNAs by CjCas9

To evaluate the collection of 96 co-purified RNA peaks for the potential to directly bind Cas9 via crRNAs, we performed MEME motif analysis (Bailey and Elkan 1994). The peaks corresponding to the tracrRNA and the four crRNAs were excluded from the motif analysis. Of the top three motifs identified in the remaining 91 sequences, two motifs displayed extensive complementarity to the ~24 nt-long spacer-derived guide portion of crRNA3 or crRNA4 (Figures 2A and S2A). These motifs were present in 15 (crRNA3 complementarity) and 51 (crRNA4 complementarity) of the 91 RNA peaks, respectively. The crRNA-complementary motifs harbored by the co-purified RNAs suggested that they are directly bound to crRNAs associated with the tracrRNA-Cas9 complex. Figures 2B, S2B, and S2C show examples of representative RNA peaks containing either motif and potential base pairing with either crRNA3 or crRNA4. Notably, the complementarity was limited to the spacer part of the crRNAs.

To further explore whether crRNA base pairing contributes to the coIP of these RNAs with the CjCas9, we used NUPACK (Zadeh et al., 2011) to predict interactions between each of the 91 identified enriched RNA peaks and each of the four crRNA guides. NUPACK allows for internal folding of complexed RNAs, reducing forced binding interactions. NUPACK predicted that 89% of the RNA peaks could potentially base pair with at least one of the crRNA guides (Figure 2C). To experimentally interrogate whether RNA peaks co-purified with CjCas9 in a crRNA-dependent manner, we deleted all but the terminal 11 nts of the crRNA3 spacer in strain NCTC11168 (Δ*crRNA3*) to disrupt this crRNA while preserving the expression and processing of crRNA4. By repeating the coIP experiment using the Cas9 3xFLAG-tagged and untagged Δ*crRNA3* strains (Figures S1B and S1C; Table S2), we found that 68% of the enriched RNA peaks predicted to preferentially bind crRNA3 in the WT coIP experiment were absent in the Δ*crRNA3* coIP experiment (Figure 2C). In contrast, only 0%–29% of the RNA peaks predicted to preferentially bind the other crRNAs were absent in

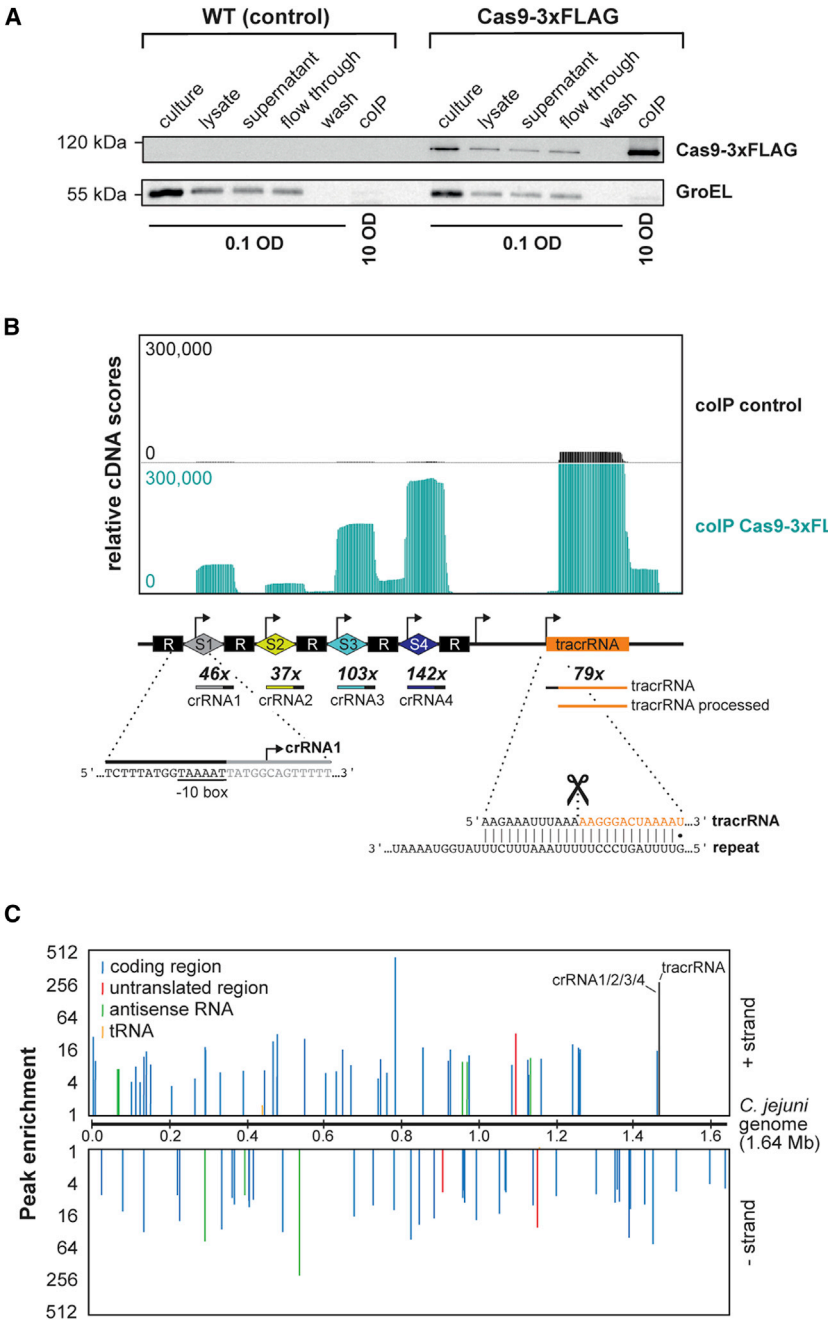

Figure 1. Cas9 Co-immunoprecipitates with Cellular RNAs in *C. jejuni*

(A) Western blot analysis of coIP samples of *C. jejuni* wild-type (WT) and *cas9*-3xFLAG strains using anti-FLAG antibody. The amount of protein samples loaded according to OD_{600} of bacteria is indicated. GroEL served as the loading control.

(B) RNA-seq reads from the control and Cas9-3xFLAG coIP libraries mapped to the CRISPR locus of *C. jejuni* strain NCTC11168. Each of the five repeats carries a -10 promoter element that drives transcription of the downstream crRNA(s). Black arrows indicate transcriptional start sites from Dugar et al., 2013. *C. jejuni* crRNAs are ~37 nt in length, with ~24 nt of spacer-derived guide sequence and ~13 nt of repeat sequence, which remains base paired with tracrRNA upon processing (Dugar et al., 2013). The sequence in orange corresponds to the processed part of the tracrRNA, and the full interaction of the crRNA repeat sequence with tracrRNA is shown below along with the RNase III-dependent cleavage site. Enrichment values of the four crRNAs and the tracrRNA are reported representing the relative reads of each RNA in the Cas9-3xFLAG coIP versus the control coIP (see also Table S2).

(C) Enrichment and genomic location of RNA peaks. CjCas9 dependent peaks were identified based on >5-fold enrichment of cDNA read counts in the Cas9-3xFLAG coIP compared to the control coIP followed by manual curation (see STAR Methods). RNA peaks are colored based on common RNA classes. The two most enriched peaks (*truA*, +775157; Cj0571 antisense, −533042) can be attributed to few reads in the control coIP (see Table S2).

in the Δ*crRNA3* coIP experiment. Figures 2B, S2B, and S2C contain representative examples of RNAs predicted to preferentially bind crRNA3 or crRNA4 that were respectively absent or present in the Cas9-3xFLAG coIP in the Δ*crRNA3* coIP experiment. For instance, an RNA peak within Cj1321 mRNA was predicted to preferentially bind crRNA3 and was not enriched in the Δ*crRNA3* Cas9-3xFLAG coIP experiment (Figure 2B). In contrast, an RNA peak within *nifU* (Cj0239c) mRNA was predicted to preferentially bind crRNA4 and was still enriched in the Δ*crRNA3* Cas9-3xFLAG coIP experiment. Of the 11 peaks preferentially bound by crRNA3 in the WT coIP that were still identified in the Δ*crRNA3* coIP experiment (Figure 2C), 3 were predicted to also base pair with crRNA4, indicating that they are potentially co-purified by crRNA4 in the absence of crRNA3. Seven peaks were predicted to base pair through the remaining 3′ 11 nt portion of the crRNA3 in the Δ*crRNA3* mutant strain more so than the peaks preferentially bound by crRNA3 in the WT coIP and absent from the Δ*crRNA3* coIP (Figure S2D). One retained peak within the *kpsM* mRNA was excluded from this analysis because the WT peak and the Δ*crRNA3* peak were offset, resulting in loss of all predicted binding sites (Table S2). These results thus provide further support for coIP of many RNAs together with CjCas9 through crRNA binding. We do note that other RNA peaks exhibited weak binding or no predicted binding to the crRNAs, suggesting that other modes of binding to CjCas9 likely remain to be discovered.

CjCas9 Directs Cleavage of Endogenous RNAs

We next sought to examine whether any of the bound RNAs are also cleaved by CjCas9, similar to crRNA-dependent cleavage

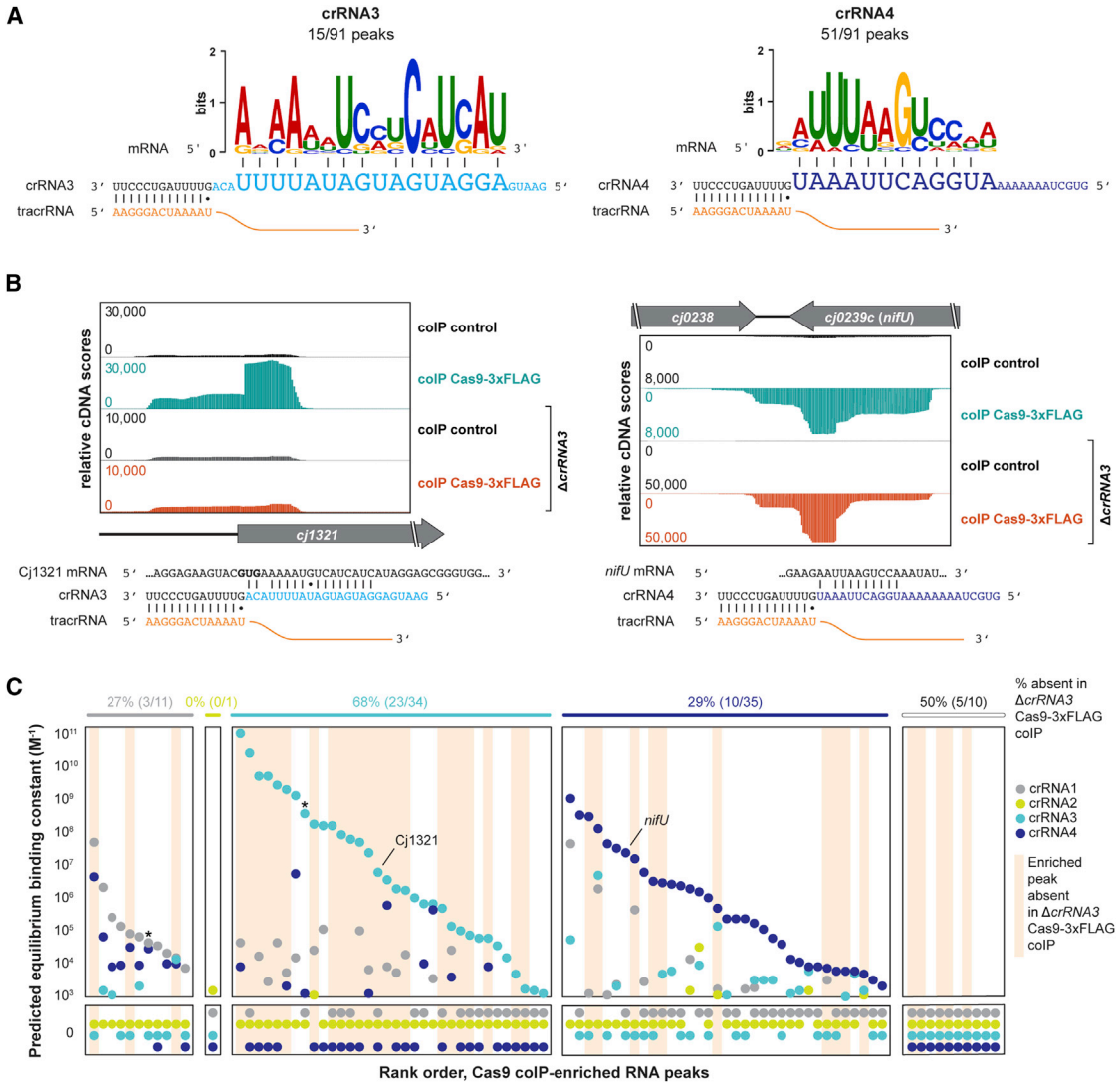

Figure 2. CjCas9 Binds Endogenous RNAs through Base Pairing with crRNAs

(A) Consensus motifs for two subsets of enriched peaks predicted by MEME. The complementarity of the respective motifs with either crRNA3 (left) or crRNA4 (right) is depicted below. Base pairing between the crRNA repeat part and tracrRNA is also shown.

(B) Examples of enriched peaks in Cj1321 mRNA and *nifU* mRNA in the Cas9-3xFLAG coIP compared to the control coIP that are predicted to base pair with crRNA3 (left, Cj1321 mRNA) or crRNA4 (right, *nifU* mRNA). The *cj1321* start codon is highlighted in bold. RNA-seq reads of the Cas9-3xFLAG coIP and the control coIP for the *C. jejuni* NCTC11168 *crRNA3*-deletion mutant are also shown.

(C) Predicted binding affinities of the enriched RNA peaks to each of the four crRNA guides predicted by NUPACK. Each dot represents the predicted binding affinity between the RNA peak and the crRNA, where the color indicates the crRNA (crRNA1, gray; crRNA2, yellow-green; crRNA3, turquoise; crRNA4, dark blue). RNA peak-crRNA pairs with no predicted base-pairing interactions appear at the bottom. RNA peaks are ordered based on the crRNA guide with the highest predicted binding affinity. RNA peaks that are not predicted to bind to any crRNA are shown on the far right. Highlighted in peach are RNA peaks that were not enriched more than 5-fold in the coIP experiment with the *crRNA3*-deletion strain. Values above each grouped set of RNA peaks indicate the percentage of RNA peaks that are highlighted in peach. Asterisks designate two RNA peaks (in the *fumC* and *kpsM* mRNAs) that shifted between the WT and Δ*crRNA3* coIP, resulting in loss of all predicted crRNA binding sites.

of double-stranded DNA substrates. Thus, we performed RNA-seq of *C. jejuni* WT as well as Δ*cas9*, Δ*CRISPR-tracrRNA*, Δ*tracrRNA*, and Δ*crRNA3* strains. To selectively determine potential Cas9-dependent cleavage sites, we visualized only the 5′ ends of the sequenced cDNA reads mapped to the genome. Comparison of the 5′ end patterns between the WT and the mutant strains revealed several potential cleavage sites within the RNA peak regions enriched in the Cas9-3xFLAG coIPs (Figure 3A). For example, potential cleavage sites were observed in Cj1321 and Cj0144 mRNAs near the 5′ end of the region complementary to crRNA3 as well as in *nifU* and Cj1302 mRNAs near the 5′ end of the region complementary to crRNA4. Comparison of the potential cleavage sites to our global transcriptional start site (TSS) map of *C. jejuni* (Dugar et al., 2013)

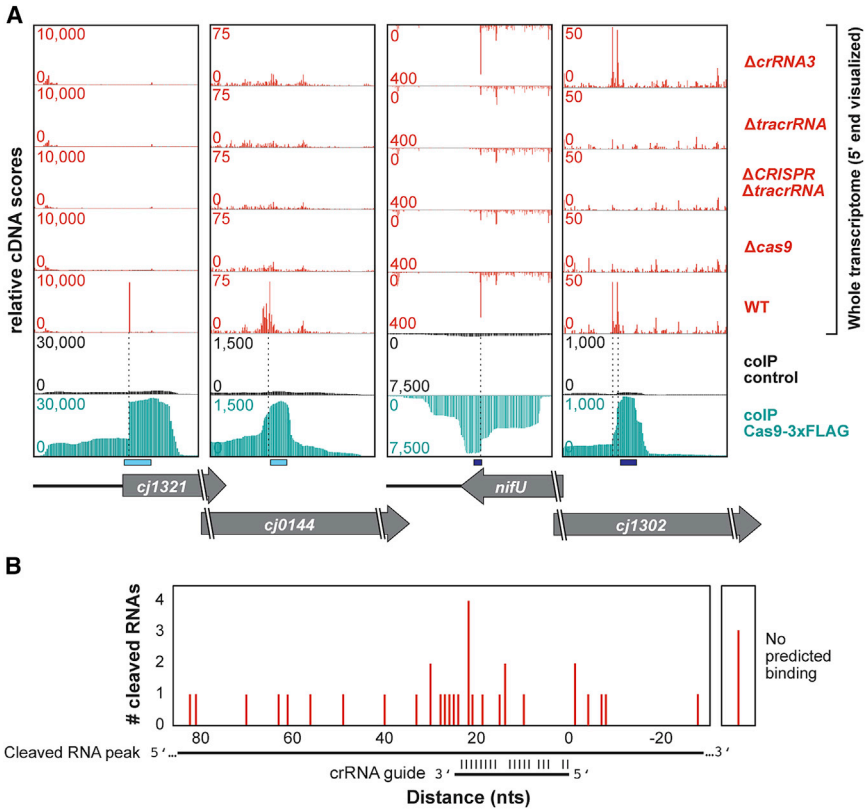

Figure 3. Some Co-purified RNAs Undergo CjCas9-Dependent Cleavage

(A) 5′ end visualization (red) of mapped cDNA reads from whole transcriptome libraries from *C. jejuni* NCTC11168 WT as well as Δ*cas9*, Δ*CRISPR-tracrRNA*, Δ*tracrRNA,* and Δ*crRNA3* mutant strains. The mapped full-length cDNA reads from the control and Cas9-3xFLAG coIP libraries are shown below. The black dotted lines mark the potential sites of Cas9-dependent mRNA cleavage. The light and dark blue boxes below indicate the predicted binding sites of crRNA3 and crRNA4, respectively.

(B) Analysis of the 35 RNA peak cleavage positions relative to the predicted crRNA binding sites. The vertical axis indicates the number of RNA peaks. The horizontal axis indicates the distance (in nucleotides) between the 5′ end of the crRNA and the cleavage site in the RNA peak. A distance of 0 corresponds to a cleavage site in the RNA peak across from the 5′ end of the crRNA. Distances were determined by counting the number of bases between the cleavage site and the closest nt base paired with the crRNA in the RNA peak, and then taking this distance relative to the 5′ end of the crRNA (see STAR Methods for details). The crRNA that bound closest to the cleavage site was selected. In all but one case, this crRNA exhibited the highest predicted binding affinity for that RNA peak. See Table S2 for binding locations and energetics. For three peaks (right), potential cleavage sites were detected but no corresponding crRNA binding sites were predicted.

confirmed that these 5′ ends represent potential cleavage sites and not TSSs. The disappearance of the putative cleavage sites upon deletion of either *cas9*, the whole CRISPR array and tracrRNA (Δ*CRISPR-tracrRNA*), or the tracrRNA alone further indicated that cleavage was dependent on these three components. In addition, while the potential cleavage site of the crRNA4 complementary sites in *nifU* and Cj1302 mRNAs were also detectable in Δ*crRNA3* strain, the potential crRNA3-dependent cleavage sites within Cj1321 and Cj0144 mRNAs disappeared.

To systematically detect the Cas9-dependent cleavage sites within the bound RNAs, we developed an automated approach. Briefly, we compared the 5′ ends between the whole transcriptomes of the WT and *cas9* deletion strains in the enriched peak regions that we had previously defined based on the coIP data (Table S2). A maximum of one cleavage site was defined per peak, given that the site was enriched in the WT library with a GFOLD (0.01) value >0 based on GFOLD differential expression analysis (Feng et al., 2012). In total, we identified 35 RNA peaks with a potential cleavage site. We next compared the putative cleavage sites with the predicted base-pairing locations of the crRNAs and identified the crRNA that base paired closest to the cleavage site. In all but one instance, this crRNA exhibited the strongest predicted binding affinity for that RNA peak; in the one exception (Cj1030c antisense), the crRNA predicted to bind closest to the cleavage site also exhibited a large equilibrium binding constant. While the cleavage sites were spread around the predicted binding site, most fell within or immediately adjacent to the site of predicted binding (Figure 3B). The site with the greatest frequency of cleavage base-paired 2 nt internal to the 3′ end of the crRNA, which is within 1 nt of the location in which Cas9 nicks both strands of target DNA. We posit that this site is cleaved directly by CjCas9, where the cleavage sites flanking the predicted binding site result from CjCas9 protecting the bound region from degradation by cellular RNases. Overall, the RNA-seq-based 5′ end analysis revealed several potential cleavage sites close to the region of crRNA complementarity, and mutational analysis confirmed that these are dependent on Cas9, crRNAs, and tracrRNA.

crRNA3-Dependent Cleavage of Cj1321 mRNA Requires the HNH Domain

We next asked if CjCas9 was directly cleaving any of the bound RNAs and focused on the enriched peak overlapping the 5′ UTR and early coding region of Cj1321 mRNA, which is encoded in an *O*-linked flagellin glycosylation island (Howard et al., 2009). This peak was selected because it was the most abundant co-purified RNA outside of the CRISPR locus (Figure 2B; Table S2) and it contained a clear crRNA3-dependent cleavage site 3 nts internal to the 3′ end of the crRNA (Figure 3A). Examination of our differential RNA-seq data of the *C. jejuni* WT strain (Dugar et al., 2013) showed that the enriched fragment corresponds to a processed fragment, as it is not detected in a terminator exonuclease (TEX)-treated cDNA library (Figure 4A). TEX degrades RNAs with a 5′-monophosphate, while primary transcripts with a 5′ PPP are not affected (Sharma et al., 2010).

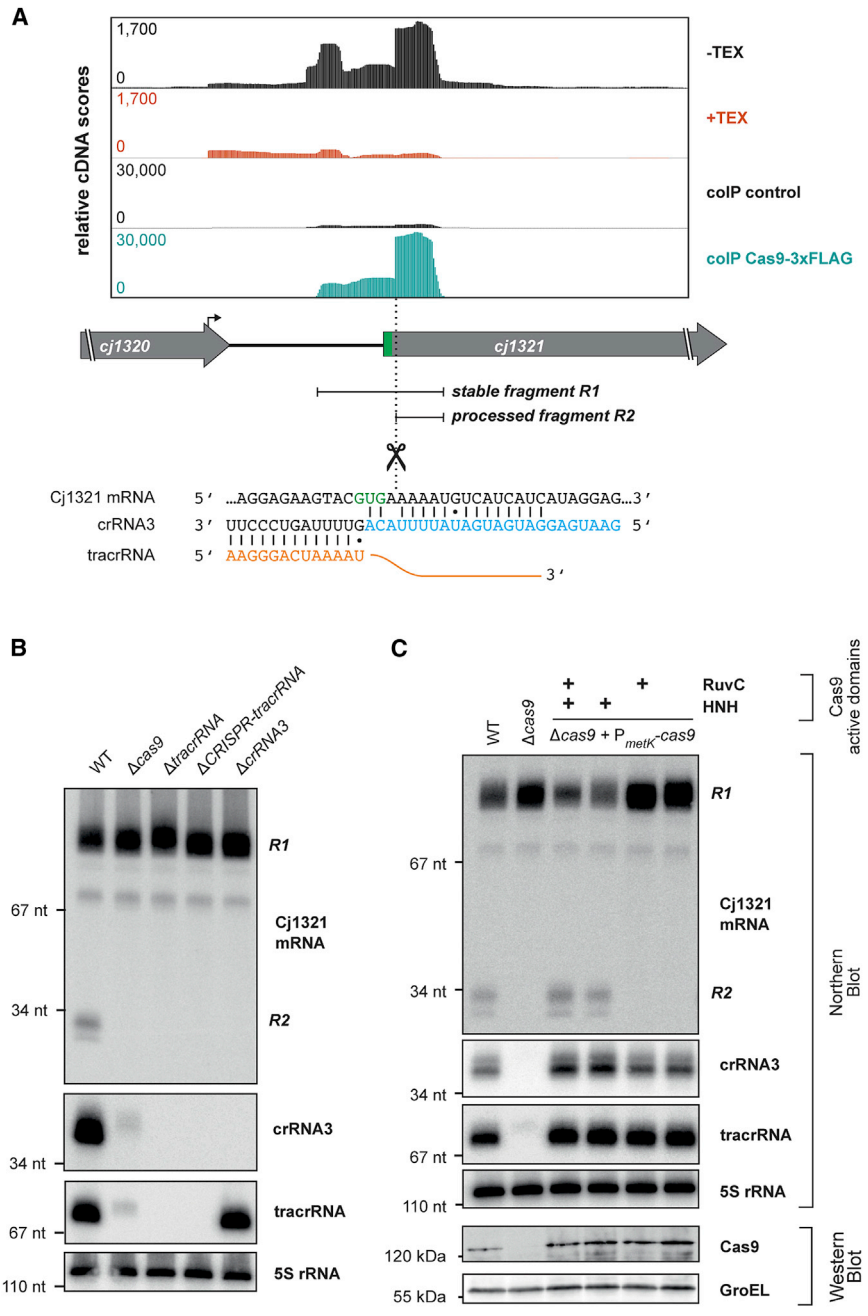

Figure 4. crRNA3-Dependent Cleavage of the Cj1321 mRNA Requires the HNH Domain of CjCas9

(A) RNA-seq reads from *C. jejuni* NCTC11168 differential RNA-seq (dRNA-seq) (Dugar et al., 2013), as well as coIP libraries mapped to the *cj1321* locus. The dRNA-seq data comprise two cDNA libraries, generated from RNA with (+TEX) or without (−TEX) prior treatment with terminator exonuclease. The two processed and stably accumulating fragments R1 and R2 of Cj1321 mRNA are indicated by black bars along with the crRNA3-Cas9-dependent cleavage site.

(B) Northern blot analysis of the Cj1321 mRNA, crRNA3, tracrRNA, and 5S rRNA in the indicated WT and CRISPR/Cas mutant strains. RNAs were probed with radiolabeled oligonucleotide probes and marker sizes are indicated on the left.

(C) Northern blot and western blot analysis of Cas9, GroEL, and RNAs mentioned in (B) in strains complementing the Δ*cas9* deletion with different nuclease mutant versions as indicated on top. Cas9 complementations are expressed under control of the P_{metK} promoter in the unrelated *rdxA* locus. "+" indicates which Cas9 nuclease domain is still intact.

While the full-length Cj1321 mRNA was not discernible on northern blots (data not shown), two stable processed fragments of Cj1321 mRNA, R1 (~90 nt) and R2 (26 nt), were detected (Figure 4B), which corresponded to the fragments observed in the RNA-seq (Figure 4A). Primer extension revealed that the 5′ end of the R1 fragment was generated by processing near a G-rich sequence (Figure S3). The R2 fragment starts one nucleotide downstream of the Cj1321 mRNA GUG start codon at the site of Cj1321 mRNA complementarity with crRNA3 (Figures 4A and S3). In line with crRNA3- and Cas9-dependent cleavage, the R2 fragment was not detectable in northern analysis of the Δ*cas9*, Δ*CRISPR-tracrRNA*, Δ*tracrRNA*, and Δ*crRNA3* strains (Figure 4B). Only the R1 fragment was still observed and was slightly more abundant (~1.8-fold) in the mutant strains. The levels of crRNA3 and the tracrRNA were strongly reduced in the Δ*cas9* strain, indicating their stabilization by Cas9. Overall, Northern analysis showed that the crRNA3-dependent cleavage of either the Cj1321 full-length mRNA or R1 fragment by Cas9 led to accumulation of the processed R2 fragment.

We used the processed R2 fragment as a readout to evaluate which of CjCas9's endonuclease domains, RuvC and/or HNH, are responsible for cleaving RNA. Normally, the HNH domain cleaves the target strand of the dsDNA protospacer that is bound by the crRNA guide, whereas the non-target strand is cleaved by the RuvC domain (Jinek et al., 2012). We complemented the *C. jejuni* Δ*cas9* strain with either Cas9 WT or Cas9 mutant variants expressed from the unrelated *metK* promoter in an ectopic locus (*rdxA*). For the Cas9 complementation mutant variants, we inactivated the RuvC (D8A), HNH (H559A), or both domains (catalytically inactive dCas9). Accumulation of the stable R2 fragment, which was lost in the Δ*cas9* mutant, was restored by complementation with WT Cas9, further confirming Cas9-mediated cleavage of Cj1321 mRNA (Figure 4C). While processing was also restored by complementation with the RuvC catalytic mutant (Figure 4C, lane 4), the R2 fragment was not detectable

upon complementation with the HNH mutant or dCas9 (Figure 4C, lanes 5 and 6). These mutational analyses revealed that cleavage of the single-stranded Cj1321 mRNA required the CjCas9 HNH domain, in line with this domain cleaving the target strand of dsDNA.

The Absence of a PAM and Perfect Complementarity to crRNA3 Prevents Cas9-Mediated Cleavage of the *cj1321* Genomic Locus

Given that CjCas9 is primarily viewed as a deoxyribonuclease, we asked why the genomic locus of *cj1321* was not undergoing cleavage. We hypothesized that two factors prevented DNA cleavage: the lack of a PAM and the lack of extensive complementarity between the crRNA3 and the DNA target. The consensus PAM for CjCas9 was originally reported as 5′-NNNNACA-3′ located on the 3′ end of the non-target strand (Fonfara et al., 2014), while more recent work has identified a requirement for a C at the +8 position (5′-NNNNACAC-3′) (Kim et al., 2017). We confirmed this PAM consensus sequence using an *in vitro* DNA cleavage assay with purified CjCas9 bound to a crRNA3 sgRNA and a dsDNA construct with perfect complementarity to the crRNA3 guide and flanked by a PAM (5′-AGAAA CAC-3′) or non-PAM (5′AGAATGTG-3′) (Figure S4A). To further interrogate the PAM, we employed a binding-based *in vivo* PAM determination assay using a 5-nt library consisting of 5′-CCNNNNNC-3′ and a catalytically inactive *C. jejuni* dCas9 (Leenay et al., 2016). The assay relies on de-repressing expression of a GFP reporter using dCas9 and then subjecting the PAM library to next-generation sequencing before and after fluorescence-activated cell sorting. The assay reproduced the canonical 5′-NNNNACAC-3′ consensus PAM but also revealed some flexibility and bias, such as against a T at position 4 or equal accommodation of a C or T at position 6 (Figure S5A). Reanalyzing an *in vitro* PAM determination assay (Kim et al., 2017) also revealed varying flexibility and bias at all positions in the PAM (Figure S5B), with the C at position 8 being the most stringent. At this site, recognition was much stronger for a C rather than the next nucleotide, T, as measured both by gene repression and a plasmid clearance assay in *E. coli* (Figures S5C and S5D). Critically, none of the identified PAMs are present upstream of the target site within the *cj1321* genetic locus.

We next interrogated whether restoring the PAM, perfect complementarity to the crRNA3 guide, or both would allow for DNA cleavage of the *cj1321* locus. We performed an *in vivo* plasmid clearance assay with CjCas9 expressed in *E. coli*, where the target plasmid encoded the *cj1321* genomic target with 10 nt of flanking genomic context or variants in which the locus was mutated to contain the consensus PAM (*cj1321* + PAM), perfect complementarity to the crRNA3 guide (*cj1321* CC), or both (*cj1321* (CC) + PAM) (Figure 5A). Cells harboring these plasmids and a plasmid expressing CjCas9 were then transformed with a third plasmid expressing an sgRNA encoding the native crRNA3 guide, and the transformation efficiency was determined in comparison to a non-targeting control sgRNA. The plasmid clearance assay showed that only the construct with perfect complementarity and a PAM sequence showed about 1,000-fold reduction in transformation efficiency compared to all other combinations and a non-targeting sgRNA.

To further confirm these DNA targeting requirements, we performed *in vitro* DNA cleavage assays of a double-stranded Cj1321 DNA fragment using purified CjCas9 complexed with sgRNAs containing different variants of the crRNA3 guide. These variants included the WT sequence (sgRNA cr3), a completely complementary sequence (sgRNA CC), and a non-targeting sequence (sgRNA NC). We tested the *cj1321* DNA target with the WT-flanking sequence or a sequence mutated to match the consensus PAM for CjCas9. The *cj1321* dsDNA target was only cleaved by CjCas9 bound to sgRNA CC with full complementarity in the presence of an NNNNACAC PAM (Figure 5B). Together, these results demonstrate why the Cj1321 locus does not undergo cleavage by CjCas9 and affirm the need for a PAM and extensive complementarity between the crRNA guide and the target for DNA cleavage.

RNA Cleavage Improves with Greater Complementarity and Is Programmable *In Vitro*

While the DNA cleavage assays confirmed PAM dependence and a requirement for full complementarity, we observed Cj1321 mRNA cleavage *in vivo* despite the absence of an obvious PAM or only partial complementarity. To further interrogate RNA cleavage, we performed *in vitro* RNA cleavage assays with recombinant CjCas9 and an sgRNA. The addition of the CjCas9 and an sgRNA with the native crRNA3 guide sequence (sgRNA cr3) (Figure 6A) was sufficient to mediate cleavage of an *in vitro* transcribed Cj1321 mRNA fragment. Mild cleavage of Cj1321 mRNA was also observed for an assay performed with crRNA3 (WT sequence) and tracrRNA, albeit with weaker cleavage than that by an sgRNA (Figure S4B). In both cases, we observed the same cleavage site detected *in vivo* just downstream of the GUG start codon of Cj1321 mRNA. No cleavage was observed when adding only one of the components Cas9, crRNA3, or tracrRNA (Figure S4B). We also investigated *in vitro* RNA cleavage by CjCas9 in the presence of sgRNAs with varying complementarity (cr3: native crRNA3 sequence with partial complementarity; CC: complete complementarity; and NC: random control sequence with no noteworthy complementarity to Cj1321 mRNA). The Cj1321 *in vitro* transcript underwent cleavage with the partially and completely complementary sgRNAs, although the efficiency was notably higher for the completely complementary sgRNA (Figures 6A and S4B).

After successful reconstitution of Cj1321 mRNA cleavage *in vitro*, we asked whether CjCas9 could be programmed to specifically cleave any RNA of interest. We designed three sgRNAs targeting an *in vitro* transcribed fragment of *C. jejuni flaA* mRNA, an unrelated RNA that was not identified as a Cas9 target in our coIP approach. The three sgRNAs (fla1, fla2, and fla3) were designed to target overlapping regions in *flaA* mRNA in steps of five nucleotides with complete complementarity. The assay showed the cleavage of the *flaA* transcript at the expected position relative to Cj1321 mRNA cleavage (Figure 6B). The cleavage products from the three sgRNAs were 5 nt apart as expected, and no cleavage was observed with the sgRNA designed with full complementarity to the Cj1321 mRNA. Overall, the *in vitro* assays showed that CjCas9-mediated RNA cleavage can be reconstituted *in vitro* and is programmable by using full-complementarity sgRNAs designed to target an RNA of choice.

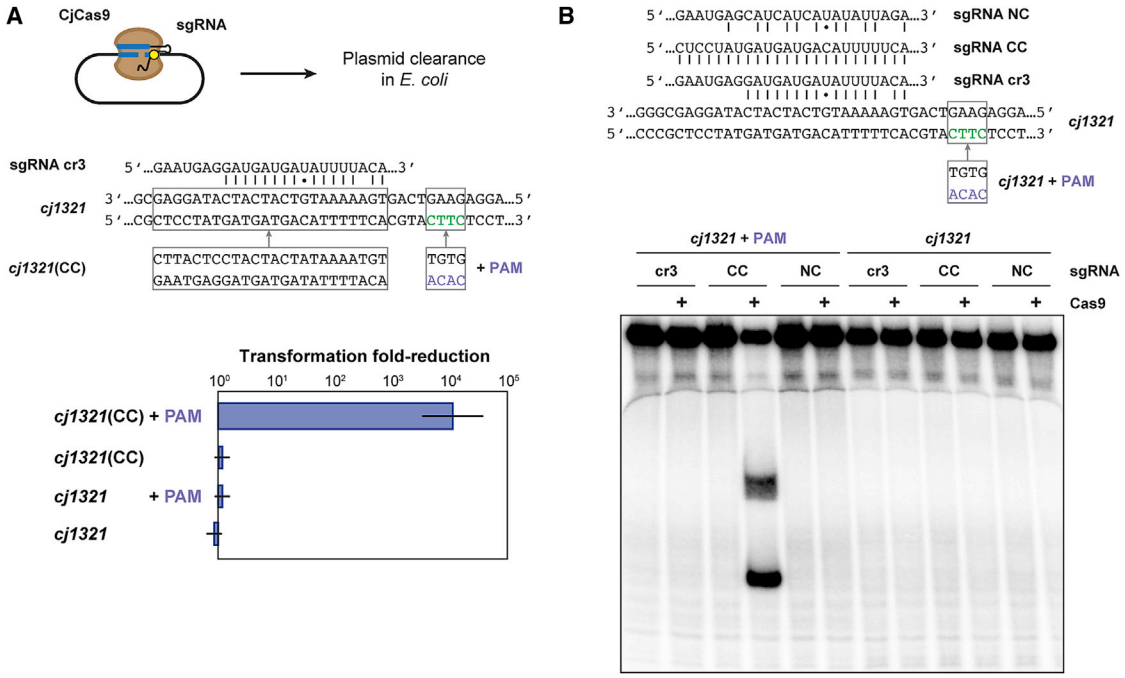

Figure 5. DNA Targeting of the Cj1321 Locus by CjCas9 Requires a PAM and Extensive crRNA Complementarity

(A) Plasmid clearance assays in *E. coli*. Assays were conducted by encoding variants of the *cj1321* locus in an *E. coli* plasmid and then measuring the transformation efficiency in cells expressing CjCas9 and the crRNA3 sgRNA or a non-targeting sgRNA. The variants included the natural locus (*cj1321*) as well as mutant variants, where the natural locus was mutated to be completely complementary to the crRNA3 guide (CC), to contain the consensus PAM (+PAM), or both. Values represent the geometric mean and SEM of experiments from three separate colonies.

(B) *In vitro cj1321* DNA cleavage assay with CjCas9 (final concentration of 300 nM). The assay was conducted for 5 min with 63 bp-long *cj1321* WT dsDNA construct or a mutant variant (final concentration of 4 nM) that includes a PAM sequence (*cj1321* + PAM). Both DNA strands are 5′ end radiolabeled. One of three sgRNAs (final concentration of 300 nM) with either no (NC), full (CC), or partial complementarity (cr3, sequence of WT crRNA3) were provided. Base-pairing interactions with *cj1321* are indicated below each sgRNA sequence. The upper cleavage fragment corresponds to the non-target strand and the lower fragment to the target strand. The results are representative of three independent experiments.

DISCUSSION

While Cas9 nucleases generally target double-stranded DNA, we found that the Cas9 from the foodborne pathogen *Campylobacter jejuni* can also target single-stranded RNA. This insight came from identification of co-immunoprecipitating RNAs bound to Cas9-3xFLAG from *C. jejuni*, which revealed that the majority of the co-purified RNAs are likely bound through base-pairing interactions with the guide portion of the CjCas9-associated crRNAs. Some of the co-purified RNAs were also cleaved by the CjCas9 through its HNH domain. Using synthetic sgRNAs with fully complementary 24 nt guides, we found that the single-stranded RNA cleavage activity of CjCas9 was programmable *in vitro*, indicating CjCas9 as a potential candidate for expanded applications of DNA/RNA targeting by Cas9.

The rules followed by CjCas9 for RNA targeting were strikingly more lenient than those for DNA targeting (Figure 6C). For instance, while DNA targeting required a defined yet somewhat flexible 3′ PAM (consensus of 5′-NNNVRYAC-3′ based on the PAM wheel), RNA targeting did not require any obvious PAM or PFS—at least based on MEME analysis and RNA cleavage *in vitro*. Nevertheless, it is possible that more systematic, global cleavage analyses of synthesized RNA pools might reveal subtle bias of CjCas9 for the target sequence. The recently reported crystal structure of CjCas9 along with an sgRNA and target dsDNA showed that, unlike other Cas9 orthologs, CjCas9 is in contact with both strands of the target DNA (Yamada et al., 2017). This additional contact between CjCas9 and the target strand of dsDNA might help explain its capability to bind and cleave single-stranded nucleic acids lacking the PAM-containing non-target strand (Ma et al., 2015). Furthermore, while DNA targeting can only accommodate some mismatches outside of the seed region, RNA targeting by CjCas9 could still occur even with limited complementarity to the guide RNA. While the majority of the co-purified RNAs in our RIP-seq analysis are likely bound through base-pairing interactions with the guide portion of the CjCas9-associated crRNAs, not all of them showed potential Cas9-dependent cleavage sites. Future studies could elucidate the exact base-pairing requirements and tolerated mismatches in the region of the guide-RNA interaction that define RNA binding or cleavage activity, and they could reveal other modes of RNA binding independent of crRNAs. It will also be interesting to compare the relative efficiencies of DNA versus RNA cleavage to determine which one is higher and, therefore, potentially the dominant mode of nuclease function.

Interestingly, the rules for RNA targeting by CjCas9 resemble those for the recently reported PAM-independent targeting of single-stranded DNA by compact Type II-C Cas9 homologs

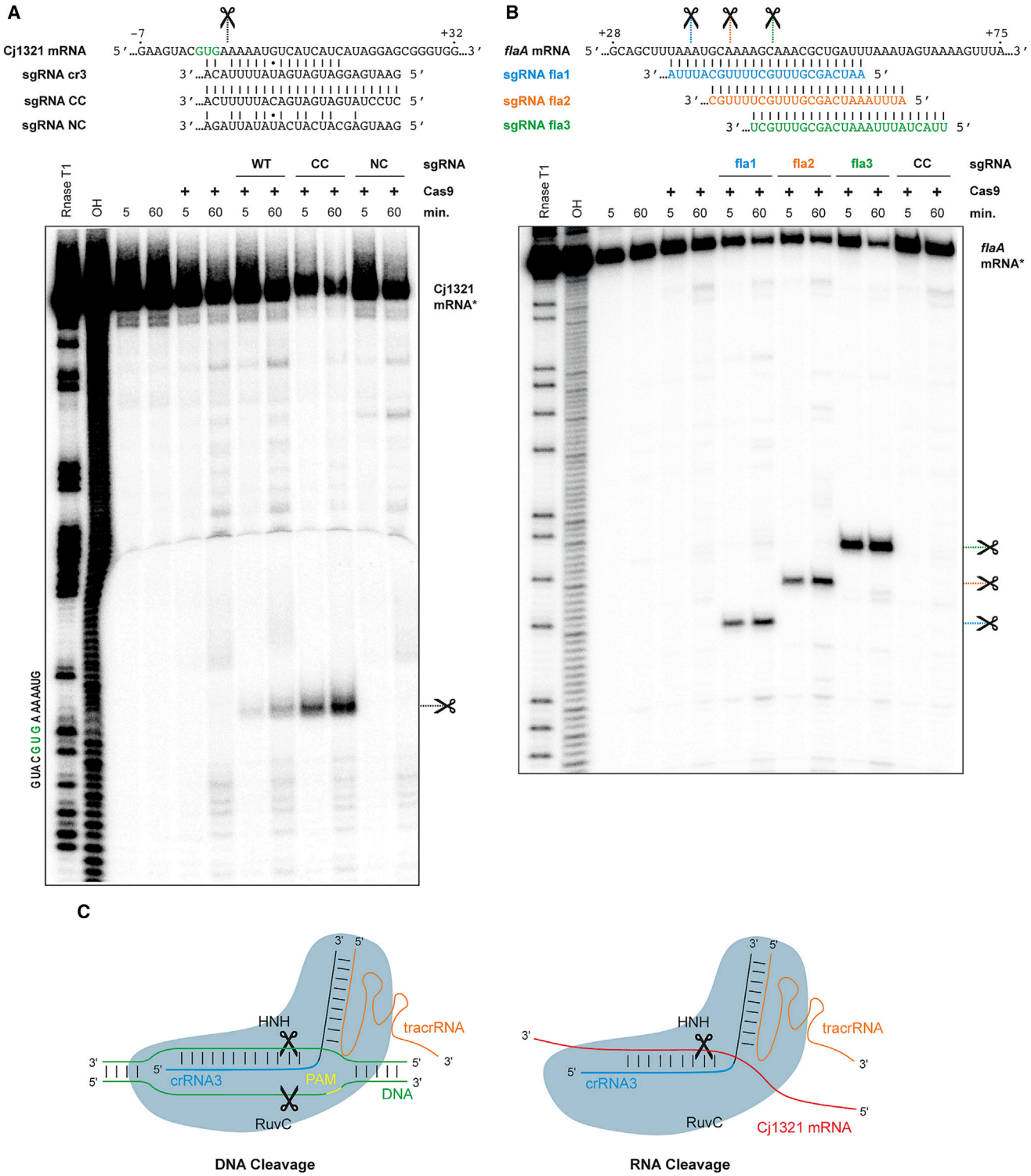

Figure 6. Enhancing and Reprogramming RNA Cleavage by CjCas9 *In Vitro*

(A) *In vitro* cleavage of 5′-end radiolabeled *in vitro*-transcribed Cj1321 mRNA (final concentration of 4 nM) with CjCas9 (final concentration of 1 μM) and guide RNAs (final concentration of 1 μM) from Figure 5B. The Cj1321 mRNA GUG start codon is marked in green, scissors indicate the cleavage site, and base-pairing interactions with the Cj1321 mRNA are indicated above each sgRNA guide. RNase T1 indicates a ladder for G residues, while OH indicates a ladder for all nucleotides. The results are representative of three independent experiments.

(legend continued on next page)

(Ma et al., 2015; Zhang et al., 2015b). While both DNase H activity by *Neisseria meningitidis* Cas9 (NmeCas9) and RNA targeting by CjCas9 required the Cas9 HNH domain and a crRNA guide, ssDNA cleavage by NmeCas9 was independent of the tracrRNA (Zhang et al., 2015b). The preferred ssDNA versus dsDNA cleavage activity of smaller Cas9 variants was attributed to their limited dsDNA binding and unwinding activity and promiscuous guide RNA specificity, which was suggested to represent an ancestral Cas9 function (Ma et al., 2015). The observed ssDNA activity of several Cas9 nucleases from the II-C subtype suggests that others might also be capable of targeting ssRNA.

The most abundantly co-purified mRNA fragment in our RIP-seq approach was derived from the *cj1321* locus. We reproducibly observed accumulation of a stable cleavage product of Cj1321 mRNA *in vivo* and could confirm Cas9-mediated Cj1321 mRNA cleavage *in vitro*. Because Cas9-mediated cleavage occurred just downstream of the GUG start codon, it might in principle lead to translational inactivation of Cj1321 mRNA. However, attempts to examine potential regulatory effects using western blot analysis of FLAG-tagged Cj1321 revealed only mild effects on protein expression under standard growth conditions (data not shown). The *cj1321* gene is part of a flagellin glycosylation gene cluster, which is characteristic of the livestock clade of *C. jejuni* strains (Champion et al., 2005; Howard et al., 2009). Genes related to flagellin modification might connect to phage infection and resistance, because flagella can be used as phage receptors. The crRNA3 spacer shows complementarity (with two mismatches) to the PC5 phage genome (Janež et al., 2014, 2016) and is also found in several other *C. jejuni* strains (Grissa et al., 2007). However, the presence of the crRNA3 spacer does not necessarily correlate with the presence of *cj1321*. Future studies will be required to understand the biogenesis and function of the R1 (~90 nt) and Cas9-mediated R2 (26 nt) cleavage products derived from the 5′ UTR and early coding region of Cj1321 mRNA. These might have a role on their own as regulatory RNAs.

For the other CjCas9-3xFLAG co-purified transcripts, it also remains unclear whether RNA targeting by CjCas9 has any physiological consequences or is just a byproduct of its DNA targeting activity. In principle, RNA targeting could be an unfortunate consequence of immune surveillance, but the limited depletion of target RNAs could have minimal effect on the cell's physiology and therefore exert negligible selective pressure. On the other hand, CjCas9 may be employed by the cell to target RNA viruses or even regulate endogenous gene expression. The acquired spacers may also evolve over time to target specific genes, similar to adaptive evolution of sRNAs along with their protein chaperone, Hfq, to target specific sets of mRNAs (Peer and Margalit, 2014). So far, we did not find any significant enrichment for functional classes of mRNAs targeted by CjCas9 (data not shown). The majority of the co-purified targets exhibited potential base-pairing interactions with crRNA3 or crRNA4, which might be explained by these two crRNAs being the most abundantly expressed crRNAs in this strain. There are emerging examples of CRISPR-Cas systems that have potential roles beyond defense and impact on diverse phenotypes such as bacterial virulence, group behavior, DNA repair, and genome evolution (Li et al., 2016; Müller-Esparza and Randau, 2017; Sampson et al., 2013, 2014; Westra et al., 2014; Zegans et al., 2009). For example, deletion of Cas9 affects virulence in several pathogens, such as *Francisella* (Sampson et al., 2013), *Neisseria* (Sampson et al., 2013), and *Campylobacter* (Louwen et al., 2013). More work will need to be done to delineate not only the prevalence of RNA targeting by Cas9 but also elucidate the different ways (if any) that RNA targeting drives cell physiology.

Cas9 has evolved as a simple yet potent RNA-based DNA targeting system that has been harnessed for gene editing. A common concern with the use of Cas9 homologs for biotechnological purposes is the potential for off-target editing through recognition of similar genomic sequences flanked by a PAM. While traditional off-target analyses focus on permanent DNA modifications (Tycko et al., 2016; Zhang et al., 2015a), our demonstration of RNA targeting by CjCas9 raises the possibility that off-target effects by Cas9 homologs could be exerted on the transcriptome. For instance, CjCas9 could bind or cleave partially complementary transcripts, resulting in perturbations of levels of the encoded proteins and their genetic networks. Furthermore, the tendency to target RNA could also reduce the overall efficiency of genome editing because Cas9 might be titrated by cellular RNAs depending on the sgRNA guide sequence. Given the potential for RNA targeting by CjCas9 and other Cas9 nucleases commonly used for genome editing, the definition and analysis of off-target effects may need to be expanded.

RNA targeting by CjCas9 also offers numerous opportunities for technological development. First, the CjCas9 has been recognized as the shortest Cas9 available for *in vivo* genome editing to date (Kim et al., 2017; Yamada et al., 2017) and could therefore offer the most compact nuclease for RNA-targeting applications (Barrangou and Gersbach, 2017; Nelles et al., 2015; Price et al., 2015). These applications of RNA targeting are broad and include RNA capture from cell lysates, RNA imaging and detection, removal of RNA microsatellites, clearing of RNA viruses, downregulation of endogenous RNAs, and site-specific chemical modification (Abudayyeh et al., 2016, 2017; Batra et al., 2017; Cox et al., 2017; East-Seletsky et al., 2017; Gootenberg et al., 2017; Nelles et al., 2016; O'Connell et al., 2014; Price et al., 2015; Smargon et al., 2017). Some of these approaches rely on catalytically inactive Type VI Cas13a/b (C2c2/C2c6) or Cas9 variants and/or fusion to RNase domains or RNA modification enzymes. The potential draw of CjCas9 beyond its small size is the lack of a PFS that confers more flexible targeting and no requirement for an accessory oligo or scaRNA. In certain organisms or for *in vitro* approaches, the ability of CjCas9 to coordinately target DNA and RNA could also be highly

(B) *In vitro* cleavage of an *in vitro*-transcribed *flaA* mRNA fragment. Three sgRNAs targeting the fragment are shown in color. The sgRNA CC with full complementarity to Cj1321 mRNA from (A) does not bind to *flaA* mRNA and serves as a control. The results are representative of two independent experiments.
(C) Model of double-stranded DNA and single-stranded RNA cleavage by CjCas9. Left: schematic drawing of dsDNA (green) cleavage (scissors) by the HNH and RuvC domains of CjCas9, which depends on the presence of a PAM (yellow) and full complementarity of the crRNA (blue) to the target strand of the dsDNA (green). Right: PAM-independent ssRNA (Cj1321, red) cleavage by the Cas9 HNH domain with partial complementarity to the crRNA3 guide (blue).

advantageous for several applications, including, for example, targeting RNA viruses such as HIV in their active and latent forms. The only other CRISPR-Cas systems reported to coordinately target DNA and RNA are the Type III systems, although these require numerous protein subunits and require the DNA to be in close proximity to the RNA (Pyenson and Marraffini, 2017). Given these possibilities, more work will need to be done to determine whether the promiscuous nucleic-acid targeting CjCas9 or other Cas nucleases are more desirable than previous RNA-targeting nucleases and which applications would benefit from a nuclease that coordinately targets DNA and RNA. Overall, the CRISPR-Cas system shows a high diversity in effector complex composition and target specificity and even within the Cas9-based Type II subtype, target specificity increasingly emerges beyond the canonical dsDNA targeting.

During the revision of this manuscript, Strutt and colleagues reported that the type II-A Cas9 from *Staphylococcus aureus* (SauCas9) and the II-C Cas9 from *C. jejuni* are capable of programmable guide-RNA-dependent targeting of single-stranded RNA *in vitro* (Strutt et al., 2018). As part of the work, the authors showed that RNA targeting was independent of a PAM and that the SauCas9 could be employed in *E. coli* for gene regulation and defense against an RNA phage. Their results complement our observation of CjCas9 binding and cleaving endogenous RNAs in its native host and further confirm that some Cas9 nucleases are naturally capable of RNA targeting and can be employed in diverse applications.

STAR★METHODS

Detailed methods are provided in the online version of this paper and include the following:

- KEY RESOURCES TABLE
- CONTACT FOR REAGENT AND RESOURCE SHARING
- METHOD DETAILS
  - Bacterial strains and plasmids
  - Oligonucleotides
  - Bacterial growth conditions
  - Construction of bacterial mutant strains
  - Construction of *C. jejuni* deletion strains
  - Construction of 3xFLAG epitope-tagged CjCas9
  - Construction of Cas9 complementation strains
  - Construction of *E. coli* CjCas9 vectors
  - RIP-seq of *Campylobacter jejuni* Cas9-3xFLAG
  - cDNA library preparation and deep sequencing
  - Analysis of RNA sequencing data
  - Peak detection and binding motif analyses
  - crRNA base-pairing predictions
  - Cas9 cleavage-site analysis
  - Base-pairing and cleavage-site comparison
  - SDS-PAGE and immunoblotting
  - RNA isolation
  - Northern blot analysis
  - *In-vitro* T7 transcription and RNA labeling
  - PAM-SCANR analysis of CjCas9
  - *E. coli* plasmid clearance assay
  - Primer extension
  - *In-vitro* DNA cleavage assay
  - *In-vitro* RNA cleavage assays
- QUANTIFICATION AND STATISTICAL ANALYSIS
- DATA AND SOFTWARE AVAILABILITY

SUPPLEMENTAL INFORMATION

Supplemental Information includes five figures and three tables and can be found with this article online at https://doi.org/10.1016/j.molcel.2018.01.032.

ACKNOWLEDGMENTS

We thank Sarah Svensson (University of Würzburg) for comments on our manuscript. We thank Emmanuelle Charpentier and Ines Fonfara (Max-Planck-Institute for Infection Biology, Berlin) for providing purified CjCas9 and Rogier Louwen (Erasmus MC, Rotterdam) for serum against CjCas9. This work was supported through funding from the Bavarian Research Network for Molecular Biosystems (BioSysNet) (to C.M.S.), the Daimler and Benz foundation (to C.M.S.), and a HIRI (Helmholtz Institute of RNA-Based Infection Research, Würzburg, Germany) seed grant (Project-No 6) through funds from the Bavarian Ministry of Economic Affairs and Media, Energy, and Technology (grant allocation numbers 0703/68674/5/2017 and 0703/89374/3/2017) (to C.M.S.), as well as the National Institutes of Health (1R35GM119561-01 to C.L.B.; 5T32GM008776-15 to R.T.L.) and the National Science Foundation (MCB-1452902 to C.L.B.). G.D. and S.K.E. were supported by a grant of the German Excellence Initiative to the Graduate School of Life Sciences, University of Würzburg.

AUTHOR CONTRIBUTIONS

Conceptualization: G.D., C.L.B., and C.M.S.; Methodology, G.D., R.T.L., T.B., C.L.B., and C.M.S.; Software: T.B.; Formal Analysis: G.D., R.T.L., T.B., C.L.B., and C.M.S.; Investigation: G.D., R.T.L., S.K.E., and B.U.A.; Writing – Original Draft: G.D., S.K.E., C.L.B., and C.M.S.; Writing – Review and Editing: G.D., R.T.L., S.K.E., T.B., C.L.B., and C.M.S.; Visualization: G.D. and C.L.B.; Supervision: C.L.B. and C.M.S.; Funding Acquisition: C.L.B. and C.M.S.

DECLARATION OF INTERESTS

C.L.B. is a co-founder and scientific advisory board member of Locus Biosciences and previously submitted provisional patent applications on CRISPR technologies.

Received: November 29, 2017
Revised: January 19, 2018
Accepted: January 24, 2018
Published: March 1, 2018

REFERENCES

Abudayyeh, O.O., Gootenberg, J.S., Konermann, S., Joung, J., Slaymaker, I.M., Cox, D.B.T., Shmakov, S., Makarova, K.S., Semenova, E., Minakhin, L., et al. (2016). C2c2 is a single-component programmable RNA-guided RNA-targeting CRISPR effector. Science *353*, aaf5573.

Abudayyeh, O.O., Gootenberg, J.S., Essletzbichler, P., Han, S., Joung, J., Belanto, J.J., Verdine, V., Cox, D.B.T., Kellner, M.J., Regev, A., et al. (2017). RNA targeting with CRISPR-Cas13. Nature *550*, 280–284.

Bailey, T.L., and Elkan, C. (1994). Fitting a mixture model by expectation maximization to discover motifs in biopolymers. Proc. Int. Conf. Intell. Syst. Mol. Biol. *2*, 28–36.

Barrangou, R., and Gersbach, C.A. (2017). Expanding the CRISPR toolbox: targeting RNA with Cas13b. Mol. Cell *65*, 582–584.

Batra, R., Nelles, D.A., Pirie, E., Blue, S.M., Marina, R.J., Wang, H., Chaim, I.A., Thomas, J.D., Zhang, N., Nguyen, V., et al. (2017). Elimination of toxic

microsatellite repeat expansion RNA by RNA-targeting Cas9. Cell *170*, 899–912.e10.

Champion, O.L., Gaunt, M.W., Gundogdu, O., Elmi, A., Witney, A.A., Hinds, J., Dorrell, N., and Wren, B.W. (2005). Comparative phylogenomics of the food-borne pathogen *Campylobacter jejuni* reveals genetic markers predictive of infection source. Proc. Natl. Acad. Sci. USA *102*, 16043–16048.

Cox, D.B.T., Gootenberg, J.S., Abudayyeh, O.O., Franklin, B., Kellner, M.J., Joung, J., and Zhang, F. (2017). RNA editing with CRISPR-Cas13. Science *358*, 1019–1027.

Deltcheva, E., Chylinski, K., Sharma, C.M., Gonzales, K., Chao, Y., Pirzada, Z.A., Eckert, M.R., Vogel, J., and Charpentier, E. (2011). CRISPR RNA maturation by trans-encoded small RNA and host factor RNase III. Nature *471*, 602–607.

Dugar, G., Herbig, A., Förstner, K.U., Heidrich, N., Reinhardt, R., Nieselt, K., and Sharma, C.M. (2013). High-resolution transcriptome maps reveal strain-specific regulatory features of multiple *Campylobacter jejuni* isolates. PLoS Genet. *9*, e1003495.

Dugar, G., Svensson, S.L., Bischler, T., Wäldchen, S., Reinhardt, R., Sauer, M., and Sharma, C.M. (2016). The CsrA-FliW network controls polar localization of the dual-function flagellin mRNA in *Campylobacter jejuni*. Nat. Commun. *7*, 11667.

East-Seletsky, A., O'Connell, M.R., Burstein, D., Knott, G.J., and Doudna, J.A. (2017). RNA targeting by functionally orthogonal type VI-A CRISPR-Cas enzymes. Mol. Cell *66*, 373–383.e3.

Edgar, R., Domrachev, M., and Lash, A.E. (2002). Gene expression omnibus: NCBI gene expression and hybridization array data repository. Nucleic Acids Res. *30*, 207–210.

Feng, J., Meyer, C.A., Wang, Q., Liu, J.S., Shirley Liu, X., and Zhang, Y. (2012). GFOLD: a generalized fold change for ranking differentially expressed genes from RNA-seq data. Bioinformatics *28*, 2782–2788.

Fonfara, I., Le Rhun, A., Chylinski, K., Makarova, K.S., Lécrivain, A.-L., Bzdrenga, J., Koonin, E.V., and Charpentier, E. (2014). Phylogeny of Cas9 determines functional exchangeability of dual-RNA and Cas9 among orthologous type II CRISPR-Cas systems. Nucleic Acids Res. *42*, 2577–2590.

Förstner, K.U., Vogel, J., and Sharma, C.M. (2014). READemption-a tool for the computational analysis of deep-sequencing-based transcriptome data. Bioinformatics *30*, 3421–3423.

Freese, N.H., Norris, D.C., and Loraine, A.E. (2016). Integrated genome browser: visual analytics platform for genomics. Bioinformatics *32*, 2089–2095.

Gasiunas, G., Barrangou, R., Horvath, P., and Siksnys, V. (2012). Cas9-crRNA ribonucleoprotein complex mediates specific DNA cleavage for adaptive immunity in bacteria. Proc. Natl. Acad. Sci. USA *109*, E2579–E2586.

Gibson, D.G., Young, L., Chuang, R.-Y., Venter, J.C., Hutchison, C.A., 3rd, and Smith, H.O. (2009). Enzymatic assembly of DNA molecules up to several hundred kilobases. Nat. Methods *6*, 343–345.

Gomaa, A.A., Klumpe, H.E., Luo, M.L., Selle, K., Barrangou, R., and Beisel, C.L. (2014). Programmable removal of bacterial strains by use of genome-targeting CRISPR-Cas systems. MBio *5*, e00928–e13.

Gootenberg, J.S., Abudayyeh, O.O., Lee, J.W., Essletzbichler, P., Dy, A.J., Joung, J., Verdine, V., Donghia, N., Daringer, N.M., Freije, C.A., et al. (2017). Nucleic acid detection with CRISPR-Cas13a/C2c2. Science *356*, 438–442.

Grissa, I., Vergnaud, G., and Pourcel, C. (2007). The CRISPRdb database and tools to display CRISPRs and to generate dictionaries of spacers and repeats. BMC Bioinformatics *8*, 172.

Hoffmann, S., Otto, C., Kurtz, S., Sharma, C.M., Khaitovich, P., Vogel, J., Stadler, P.F., and Hackermüller, J. (2009). Fast mapping of short sequences with mismatches, insertions and deletions using index structures. PLoS Comput. Biol. *5*, e1000502.

Howard, S.L., Jagannathan, A., Soo, E.C., Hui, J.P.M., Aubry, A.J., Ahmed, I., Karlyshev, A., Kelly, J.F., Jones, M.A., Stevens, M.P., et al. (2009). *Campylobacter jejuni* glycosylation island important in cell charge, legionaminic acid biosynthesis, and colonization of chickens. Infect. Immun. *77*, 2544–2556.

Janež, N., Kokošin, A., Zaletel, E., Vranac, T., Kovač, J., Vučković, D., Smole Možina, S., Curin Šerbec, V., Zhang, Q., Accetto, T., et al. (2014). Identification and characterisation of new *Campylobacter* group III phages of animal origin. FEMS Microbiol. Lett. *359*, 64–71.

Janež, N., Peterka, M., and Accetto, T. (2016). Complete genome sequences of group III *Campylobacter* bacteriophages PC5 and PC14. Genome Announc. *4*, e01030-16.

Jiang, F., and Doudna, J.A. (2017). CRISPR-Cas9 structures and mechanisms. Annu. Rev. Biophys. *46*, 505–529.

Jinek, M., Chylinski, K., Fonfara, I., Hauer, M., Doudna, J.A., and Charpentier, E. (2012). A programmable dual-RNA-guided DNA endonuclease in adaptive bacterial immunity. Science *337*, 816–821.

Kim, E., Koo, T., Park, S.W., Kim, D., Kim, K., Cho, H.-Y., Song, D.W., Lee, K.J., Jung, M.H., Kim, S., et al. (2017). In vivo genome editing with a small Cas9 orthologue derived from *Campylobacter jejuni*. Nat. Commun. *8*, 14500.

Koonin, E.V., Makarova, K.S., and Zhang, F. (2017). Diversity, classification and evolution of CRISPR-Cas systems. Curr. Opin. Microbiol. *37*, 67–78.

Leenay, R.T., and Beisel, C.L. (2017). Deciphering, communicating, and engineering the CRISPR PAM. J. Mol. Biol. *429*, 177–191.

Leenay, R.T., Maksimchuk, K.R., Slotkowski, R.A., Agrawal, R.N., Gomaa, A.A., Briner, A.E., Barrangou, R., and Beisel, C.L. (2016). Identifying and visualizing functional PAM diversity across CRISPR-Cas systems. Mol. Cell *62*, 137–147.

Li, R., Fang, L., Tan, S., Yu, M., Li, X., He, S., Wei, Y., Li, G., Jiang, J., and Wu, M. (2016). Type I CRISPR-Cas targets endogenous genes and regulates virulence to evade mammalian host immunity. Cell Res. *26*, 1273–1287.

Louwen, R., Horst-Kreft, D., de Boer, A.G., van der Graaf, L., de Knegt, G., Hamersma, M., Heikema, A.P., Timms, A.R., Jacobs, B.C., Wagenaar, J.A., et al. (2013). A novel link between *Campylobacter jejuni* bacteriophage defence, virulence and Guillain-Barré syndrome. Eur. J. Clin. Microbiol. Infect. Dis. *32*, 207–226.

Love, M.I., Huber, W., and Anders, S. (2014). Moderated estimation of fold change and dispersion for RNA-seq data with DESeq2. Genome Biol. *15*, 550.

Ma, E., Harrington, L.B., O'Connell, M.R., Zhou, K., and Doudna, J.A. (2015). Single-stranded DNA cleavage by divergent CRISPR-Cas9 enzymes. Mol. Cell *60*, 398–407.

Makarova, K.S., Wolf, Y.I., Alkhnbashi, O.S., Costa, F., Shah, S.A., Saunders, S.J., Barrangou, R., Brouns, S.J.J., Charpentier, E., Haft, D.H., et al. (2015). An updated evolutionary classification of CRISPR-Cas systems. Nat. Rev. Microbiol. *13*, 722–736.

Marraffini, L.A. (2015). CRISPR-Cas immunity in prokaryotes. Nature *526*, 55–61.

Mohanraju, P., Makarova, K.S., Zetsche, B., Zhang, F., Koonin, E.V., and van der Oost, J. (2016). Diverse evolutionary roots and mechanistic variations of the CRISPR-Cas systems. Science *353*, aad5147.

Müller-Esparza, H., and Randau, L. (2017). Commentary: Type I CRISPR-Cas targets endogenous genes and regulates virulence to evade mammalian host immunity. Front. Microbiol. *8*, 319.

Nelles, D.A., Fang, M.Y., Aigner, S., and Yeo, G.W. (2015). Applications of Cas9 as an RNA-programmed RNA-binding protein. BioEssays *37*, 732–739.

Nelles, D.A., Fang, M.Y., O'Connell, M.R., Xu, J.L., Markmiller, S.J., Doudna, J.A., and Yeo, G.W. (2016). Programmable RNA tracking in live cells with CRISPR/Cas9. Cell *165*, 488–496.

O'Connell, M.R., Oakes, B.L., Sternberg, S.H., East-Seletsky, A., Kaplan, M., and Doudna, J.A. (2014). Programmable RNA recognition and cleavage by CRISPR/Cas9. Nature *516*, 263–266.

Ondov, B.D., Bergman, N.H., and Phillippy, A.M. (2011). Interactive metagenomic visualization in a web browser. BMC Bioinformatics *12*, 385.

Peer, A., and Margalit, H. (2014). Evolutionary patterns of *Escherichia coli* small RNAs and their regulatory interactions. RNA *20*, 994–1003.

Price, A.A., Sampson, T.R., Ratner, H.K., Grakoui, A., and Weiss, D.S. (2015). Cas9-mediated targeting of viral RNA in eukaryotic cells. Proc. Natl. Acad. Sci. USA *112*, 6164–6169.

Pyenson, N.C., and Marraffini, L.A. (2017). Type III CRISPR-Cas systems: when DNA cleavage just isn't enough. Curr. Opin. Microbiol. *37*, 150–154.

Ran, F.A., Cong, L., Yan, W.X., Scott, D.A., Gootenberg, J.S., Kriz, A.J., Zetsche, B., Shalem, O., Wu, X., Makarova, K.S., et al. (2015). In vivo genome editing using *Staphylococcus aureus* Cas9. Nature *520*, 186–191.

Rieder, R., Reinhardt, R., Sharma, C., and Vogel, J. (2012). Experimental tools to identify RNA-protein interactions in *Helicobacter pylori*. RNA Biol. *9*, 520–531.

Sampson, T.R., Saroj, S.D., Llewellyn, A.C., Tzeng, Y.-L., and Weiss, D.S. (2013). A CRISPR/Cas system mediates bacterial innate immune evasion and virulence. Nature *497*, 254–257.

Sampson, T.R., Napier, B.A., Schroeder, M.R., Louwen, R., Zhao, J., Chin, C.-Y., Ratner, H.K., Llewellyn, A.C., Jones, C.L., Laroui, H., et al. (2014). A CRISPR-Cas system enhances envelope integrity mediating antibiotic resistance and inflammasome evasion. Proc. Natl. Acad. Sci. USA *111*, 11163–11168.

Sharma, C.M., Hoffmann, S., Darfeuille, F., Reignier, J., Findeiss, S., Sittka, A., Chabas, S., Reiche, K., Hackermüller, J., Reinhardt, R., et al. (2010). The primary transcriptome of the major human pathogen *Helicobacter pylori*. Nature *464*, 250–255.

Sittka, A., Lucchini, S., Papenfort, K., Sharma, C.M., Rolle, K., Binnewies, T.T., Hinton, J.C.D., and Vogel, J. (2008). Deep sequencing analysis of small noncoding RNA and mRNA targets of the global post-transcriptional regulator, Hfq. PLoS Genet. *4*, e1000163.

Smargon, A.A., Cox, D.B.T., Pyzocha, N.K., Zheng, K., Slaymaker, I.M., Gootenberg, J.S., Abudayyeh, O.A., Essletzbichler, P., Shmakov, S., Makarova, K.S., et al. (2017). Cas13b is a type VI-B CRISPR-associated RNA-guided RNase differentially regulated by accessory proteins Csx27 and Csx28. Mol. Cell *65*, 618–630.e7.

Strutt, S.C., Torrez, R.M., Kaya, E., Negrete, O.A., and Doudna, J.A. (2018). RNA-dependent RNA targeting by CRISPR-Cas9. eLife *7*, e32724.

Tycko, J., Myer, V.E., and Hsu, P.D. (2016). Methods for optimizing CRISPR-Cas9 genome editing specificity. Mol. Cell *63*, 355–370.

Westra, E.R., Buckling, A., and Fineran, P.C. (2014). CRISPR-Cas systems: beyond adaptive immunity. Nat. Rev. Microbiol. *12*, 317–326.

Yamada, M., Watanabe, Y., Gootenberg, J.S., Hirano, H., Ran, F.A., Nakane, T., Ishitani, R., Zhang, F., Nishimasu, H., and Nureki, O. (2017). Crystal structure of the minimal Cas9 from *Campylobacter jejuni* reveals the molecular diversity in the CRISPR-Cas9 systems. Mol. Cell *65*, 1109–1121.e3.

Zadeh, J.N., Steenberg, C.D., Bois, J.S., Wolfe, B.R., Pierce, M.B., Khan, A.R., Dirks, R.M., and Pierce, N.A. (2011). NUPACK: Analysis and design of nucleic acid systems. J. Comput. Chem. *32*, 170–173.

Zaslaver, A., Bren, A., Ronen, M., Itzkovitz, S., Kikoin, I., Shavit, S., Liebermeister, W., Surette, M.G., and Alon, U. (2006). A comprehensive library of fluorescent transcriptional reporters for *Escherichia coli*. Nat. Methods *3*, 623–628.

Zegans, M.E., Wagner, J.C., Cady, K.C., Murphy, D.M., Hammond, J.H., and O'Toole, G.A. (2009). Interaction between bacteriophage DMS3 and host CRISPR region inhibits group behaviors of *Pseudomonas aeruginosa*. J. Bacteriol. *191*, 210–219.

Zhang, Y., Heidrich, N., Ampattu, B.J., Gunderson, C.W., Seifert, H.S., Schoen, C., Vogel, J., and Sontheimer, E.J. (2013). Processing-independent CRISPR RNAs limit natural transformation in *Neisseria meningitidis*. Mol. Cell *50*, 488–503.

Zhang, X.-H., Tee, L.Y., Wang, X.-G., Huang, Q.-S., and Yang, S.-H. (2015a). Off-target effects in CRISPR/Cas9-mediated genome engineering. Mol. Ther. Nucleic Acids *4*, e264.

Zhang, Y., Rajan, R., Seifert, H.S., Mondragón, A., and Sontheimer, E.J. (2015b). DNase H activity of *Neisseria meningitidis* Cas9. Mol. Cell *60*, 242–255.

STAR★METHODS

KEY RESOURCES TABLE

REAGENT or RESOURCE	SOURCE	IDENTIFIER
Antibodies		
Monoclonal ANTI-FLAG M2 antibody	Sigma-Aldrich	Cat# F1804, RRID: AB_262044
Sheep Anti-Mouse IgG	GE-Healthcare	Cat# RPN4201
Anti-Cas9 serum	Louwen et al., 2013	N/A
Goat Anti-Rabbit IgG	GE-Healthcare	Cat# RPN4301, RRID: AB_2650489
Anti-GroEL antibody	Sigma-Aldrich	Cat# G6532, RRID: AB_259939
Bacterial and Virus Strains		
For bacterial strains see Table S3	N/A	N/A
Chemicals, Peptides, and Recombinant Proteins		
Protein A-Sepharose	Sigma-Aldrich	Cat# P6649
CjCas9	Emmanuelle Charpentier, Max-Planck-Institute for Infection Biology, Berlin	N/A
Critical Commercial Assays		
MEGAscript T7 kit	Ambion	Cat# AM1334
SequiTherm EXCEL II DNA Sequencing Kit	Epicenter Biotechnologies	Cat# SE9101LC
Deposited Data		
Raw and analyzed data	This paper	GEO: GSE106849
Raw Gel Images	This paper	https://doi.org/10.17632/r9sc7f3ybv.1
Oligonucleotides		
For oligonucleotides see Table S3	N/A	N/A
Recombinant DNA		
For plasmids and GBlocks see Table S3	N/A	N/A
Software and Algorithms		
FASTX toolkit	N/A	http://hannonlab.cshl.edu/fastx_toolkit/
READemption	Förstner et al., 2014	https://pythonhosted.org/READemption/
segemehl	Hoffmann et al., 2009	http://www.bioinf.uni-leipzig.de/Software/segemehl/
DESeq2	Love et al., 2014	http://bioconductor.org/packages/release/bioc/html/DESeq2.html
Integrated Genome Browser (IGB)	Freese et al., 2016	http://bioviz.org/igb/
sliding_window_peak_calling_script	Dugar et al., 2016	https://doi.org/10.5281/zenodo.49292
MEME	Bailey and Elkan, 1994	http://meme-suite.org/tools/meme
GFOLD	Feng et al., 2012	
Krona software package	Ondov et al., 2011	https://github.com/marbl/Krona/wiki
NUPACK	Zadeh et al., 2011	http://www.nupack.org/

CONTACT FOR REAGENT AND RESOURCE SHARING

Further information and requests for resources and reagents should be directed to and will be fulfilled by the Lead Contact, Cynthia Sharma (cynthia.sharma@uni-wuerzburg.de).

METHOD DETAILS

Bacterial strains and plasmids

All *C. jejuni* and *E. coli* strains and plasmids used in this study are listed in Table S3.

Oligonucleotides

All oligonucleotides used in this study are listed in Table S3.

Bacterial growth conditions

C. jejuni strains were routinely grown on Müller-Hinton agar plates or with shaking in Brucella broth (BB), both supplemented with 10 μg/ml vancomycin, at 37°C under microaerobic (10% CO_2, 5% O_2) conditions as described previously (Dugar et al., 2013). The agar was further supplemented with marker-selective antibiotics (kanamycin 50 μg/ml, chloramphenicol 20 μg/ml, or hygromycin B 250 μg/ml) where appropriate. *E. coli* strains were grown aerobically at 37°C in Luria-Bertani (LB) medium supplemented with the appropriate antibiotics.

Construction of bacterial mutant strains

All *C. jejuni* mutant strains (deletion, chromosomal 3xFLAG-tagging and complementations) were constructed using double-cross-over homologous recombination as previously described (Dugar et al., 2016). Oligonucleotides used to amplify regions of upstream/downstream homology and resistance cassettes for homologous recombination, as well as recipient strains and oligonucleotides for validation of mutant strains by colony PCR, are listed in Table S3 for each generated strain. Introduction of PCR products with 500 bp homologous ends or genomic DNA with mutant constructs into *C. jejuni* was performed by electroporation or natural transformation, respectively, as described previously (Dugar et al., 2013).

Construction of *C. jejuni* deletion strains

All *C. jejuni* deletion mutant strains listed in Table S3 were generated by double-crossover homologous recombination with PCR products of deletion cassettes that were constructed by overlap PCR (for details see Table S3) and electroporated into bacteria as described above. PCR products carried the *aphA-3* kanamycin, *C. coli cat* chloramphenicol or *aph*(7″) hygromycin resistance cassettes flanked by ~500 bp of homologous sequence up- and downstream of the target region to be deleted as previously described (Dugar et al., 2016).

As an example, the construction of the *C. jejuni* NCTC11168 Δ*cas9*::Kan^R deletion mutant is described. About 500 bp upstream of the *cas9* (*cj1523c*) start codon was amplified from genomic DNA (gDNA) of *C. jejuni* NCTC11168 WT using 'UP' primers (CSO-0802/-0803). Likewise, ~500 bp downstream of the *cas9* stop codon was amplified using 'DN' primers (CSO-0804/-0805). The 5′ ends of the antisense-UP primer (CSO-0802) and sense-DN primer (CSO-0805) contained ~25 bp of sequence homologous to the sense or antisense primer (HPK1/HPK2), respectively, used to amplify the non-polar *aphA-3* resistance cassette. PCR products were purified (Macherey-Nagel NucleoSpin PCR cleanup kit), and UP, DN, and resistance cassette amplicons were then added together in a ratio of 50:50:90 ng to a 100 μl Phusion polymerase PCR reaction with sense-UP and antisense-DN primers (CSO-0803/-0804) at a final concentration of 0.06 μM. Overlap PCR was performed with the following conditions: 1 cycle of [98°C, 3 min; 61°C, 1 min; 72°C, 10 min; 98°C, 1 min], 40 cycles of [98°C, 15 s; 57°C, 20 s; 72°C, 3 min], followed by a 10 min final extension at 72°C. Following verification of product size by agarose gel electrophoresis and purification (Macherey-Nagel NucleoSpin PCR cleanup kit), the resulting overlap PCR product was electroporated into the appropriate recipient *C. jejuni* strain. Deletion mutants for *crRNA3*::Cm^R, *tracrRNA*::Cm^R, *CRISPR-tracrRNA*::Cm^R and *cas9*::Hyg^R were constructed similarly by insertion of *cat* or *aph*(7″) resistance cassettes. Briefly, the whole sequence of *tracrRNA* was deleted by insertion of a *cat* cassette that is transcribed from the retained tracrRNA promoter and contains a transcriptional terminator sequence. The whole sequence of CRISPR-*tracrRNA* was deleted by insertion of the *cat* cassette containing a promoter and terminator sequence. *crRNA3* was partly deleted by inserting a non-polar *cat* resistance cassette in the middle of the spacer and, thereby, replacing eight base pairs (AGGATGAT) from the crRNA 3 spacer part (GAATGAGGATGATGATATTTTACA) (see Table S3). DMSO (3% final) was also added to any reactions involving amplification of *aph*(7″).

Construction of 3xFLAG epitope-tagged CjCas9

C. jejuni Cas9 was fused to a 3xFLAG epitope at its C terminus by cloning the region encoding ~500 bp of its C-terminal coding region (C-term) and ~500 bp downstream of the stop codon (DN) into plasmid pGG1 to flank a 3xFLAG tag and Kan^R cassette. Afterwards, the 3xFLAG-tag construct was amplified by PCR and introduced into the chromosome of *C. jejuni* by electroporation and double-crossover homologous recombination. Approximately 500 bp of the region downstream of *cas9* was amplified from gDNA with primers CSO-0376/-0377. These primers included EcoRI and *Xba*I sites, respectively. Following cleanup, the PCR product was digested with EcoRI and *Xba*I and ligated into a similarly-digested pGG1 backbone, generated by inverse PCR with primers CSO-0074/-0075, to create pGD12-1. The plasmid was verified by colony PCR with primers JVO-0054/CSO-0173 and sequence verified using JVO-0054. Next, the backbone of this plasmid, including the *cas9* "DN" region, was amplified by PCR with primers CSO-0073 (*Xho*I) and JVO-5142 (blunt). The C-terminal coding region of *cas9* (~500 bp) without the stop codon was amplified with primers CSO-0374/-0375 from NCTC11168 WT gDNA. The sense primer (CSO-0374) included an *Xho*I site, whereas the antisense primer (CSO-0375) contained a 5′-phosphate. Both the plasmid backbone with the "DN" insert and the C-term insert were digested with *Xho*I and ligated to create plasmid pGD19-1. Integration of the PCR product was confirmed by colony PCR using primers CSO-0374/-0023 and the plasmid was validated by sequencing using CSO-0023. The entire integration cassette was then amplified with Phusion polymerase (NEB) using primers CSO-0374/-0377 and electroporated into *C. jejuni* and selected on kanamycin plates.

Mutants were confirmed by colony PCR with primers CSO-0373/-0023 and western blot analysis with an anti-FLAG antibody (RRID: AB_262044).

Construction of Cas9 complementation strains

The *cas9* gene (from second codon to stop codon) was amplified from *C. jejuni* NCTC11168 gDNA using oligos CSO-2769/-2770. CSO-2769 introduced an *Nsi*I (ATGCAT) site which also acted as a start codon for the *cas9* gene, and CSO-2770 introduced a PstI site for cloning. The *Campylobacter* complementation plasmid pST1-1 (used for introduction of *gfpM3* under control of the *metK* promoter in the *rdxA* locus of NCTC11168 using a Kan^R cassette) was amplified using the oligos CSO-760/-0493 to replace GfpM3 with the amplified *cas9* gene resulting in plasmid pGD116-1. The construct was then amplified using oligos CSO-2276/-2277 and introduced into the *rdxA* locus of *C. jejuni* NCTC11168 *cas9*::Hyg^R.

Mutations were then introduced into the *cas9* sequence by inverse PCR on pGD116-1 using complementary oligos harboring the desired mutation, followed by *Dpn*I digestion and transformation of the resulting purified PCR product into *E. coli* TOP10. For introduction of the HNH mutation (H559A), HNH-sense / HNH-antisense oligonucleotides were used for inverse PCR on pGD116-1. The mutation was confirmed in the resulting plasmid pGD210-2. Similarly, the RuvC mutation (D8A) was introduced using primer pairs CSO-2858/-3083 resulting in plasmid pGD220-2. For combination of both HNH and RuvC mutations, a similar mutagenesis approach was performed based on PCR amplification of the pGD210-2 plasmid using oligonucleotides CSO-2858/-3083, resulting in pGD217-2 harboring both the mutations. The constructs were then amplified using oligos CSO-2276/-2277 and introduced in the *rdxA* locus of *C. jejuni* NCTC11168 *cas9*::Hyg^R.

Construction of *E. coli* CjCas9 vectors

All cloning was performed in *E. coli* NovaBlue (pCB405) or NEB 5-alpha chemically competent cells from NEB (NEB CN#E0554S). For WT *C. jejuni* Cas9, plasmid pSE59-1 was used. This plasmid was constructed by exchanging the kanamycin resistance cassette with the chloramphenicol resistance cassette in pGD116-1. The *cat* cassette from *C. coli* was amplified using CSO-2989/-2990, the plasmid was amplified with CSO-0482/-0759 based on pGD116-1. Both parts were digested with XmaI and *Not*I, ligated, and introduced into *E. coli* TOP10. Based on the verified plasmid pSE59-1, HNH-, RuvC-, and a double mutant were constructed as described above for the kanamycin constructs. Both the active Cas9 and dCas9 were amplified using oRL5-6 and oRL1-2 respectively, and digested with XmaI and PstI. A pBAD33 backbone was also digested with the same enzymes and the pieces were stitched together using T4 DNA Ligase (NEB CN#M0202S). To ensure constitutive expression, a constitutive, synthetic J23108 promoter was inserted upstream of both Cas9 variants by phosphorylating oligos oRL3-4 using T4 PNK (NEB CN#M0201S), annealing them, and ligating them into each Cas9 backbone after digestion with *Nsi*I and *Sac*I. This formed Campy_dCas9_pBad33_J23108 and Campy_Cas9_pBad33_J23108. A codon optimized version of this Cas9 was also synthesized (Genscript_COCas9) and inserted into pBAD33 with Gibson cloning (Gibson et al., 2009) (NEB CN#E2611S) using oRL7-8.

To create the sgRNA construct for targeting, a gBlock was synthesized (Campy_Bbs1_sgRNA) that contained internal BbsI cut sites, allowing for insertion of any desired spacer sequence. This was inserted into pcrRNA.con between a J23119 synthetic promoter and a terminator using Gibson cloning (Gibson et al., 2009) and oRL15-16. The codon optimized Cas9 backbone also contained this construct, allowing for a single-vector system when utilizing this version of Cas9. The spacer taken from the endogenous crRNA3 (oRL9-10), a spacer targeting the PAM-SCANR genetic circuit (oRL19-20) (Leenay et al., 2016), and a spacer targeting a GFP reporter gene (oRL17-18) (Leenay et al., 2016) were all inserted into this sgRNA backbone by first phosphorylating the oligos and annealing them as described previously. These were then inserted into the *Bbs*I-digested backbone. To also create a single-vector targeting system for the WT *C. jejuni* Cas9, these created targeting sgRNA circuits were inserted into the backbone of the Cas9 using oRL13-14 (Gibson et al., 2009).

To create targeting vectors for plasmid clearance mimicking the endogenous *cj1321* locus, p66-*lacZ* (Zaslaver et al., 2006) was digested with *Xho*I and *Aat*II and oRL21-28 were phosphorylated, annealed, and ligated into this backbone. To form the target for transcriptional repression, recognized PAM sequences were inserted into p66-*lacZ* using oRL29-32 using Q5 site-directed mutagenesis (NEB CN#E0554S). The ACAG PAM in the endogenous *cj1321* locus experiment was replaced with a ACAC PAM also using Q5 mutagenesis and oRL33-34.

RIP-seq of *Campylobacter jejuni* Cas9-3xFLAG

Co-immunoprecipitation (coIP) combined with RNA-seq (RIP-seq) to identify direct RNA binding partners of Cas9-3xFLAG in *C. jejuni* was performed as previously described (Rieder et al., 2012; Dugar et al., 2016) with minor modifications.

CoIP of chromosomally epitope-tagged *C. jejuni* Cas9 with an anti-FLAG antibody and Protein A-Sepharose beads was performed from lysates of *C. jejuni* NCTC11168 WT and Δ*crRNA3* (control) and the corresponding tagged *cas9*-3xFLAG strains grown in 100 mL (50 mL x 2 flasks) Brucella broth containing 10 μg/mL vancomycin to mid-exponential phase (OD_{600} = 0.6) at 37°C. Cells were harvested by centrifugation at 6000 x g for 15 min at 4°C. Afterwards, cell pellets were resuspended in 1 mL Buffer A (20 mM Tris-HCl, pH 8.0, 150 mM KCl, 1 mM $MgCl_2$, 1 mM DTT) and subsequently centrifuged (3 min, 11,000 x g, 4°C). The pellets were shock-frozen in liquid nitrogen and stored at −80°C. Frozen pellets were thawed on ice and resuspended in 0.8 mL Buffer A. An equal volume of glass beads was then added to the cell suspension. Cells were then lysed using a Retsch MM40 ball mill (30 s^{-1}, 10 min) in pre-cooled blocks (4°C), and centrifuged for 2 min at 15,200 x g, 4°C. The supernatant was transferred to a new tube, and an additional

0.4 mL of Buffer A was added to the remaining unlysed cells with beads. Lysis of the remaining cells was achieved by a second round of lysis at 30 s^{-1} for 5 min. Centrifugation was repeated and this second supernatant was combined with the first one. The combined supernatant was centrifuged again for 30 min at 15,200 x g, 4°C for clarification and the resulting supernatant (lysate fraction) was transferred to a new tube. The lysate was incubated with 35 μL anti-FLAG antibody (Monoclonal ANTI-FLAG M2, Sigma, #F 1804, RRID: AB_262044) for 30' at 4°C on a rocker. Next, 75 μL of Protein A-Sepharose (Sigma, #P6649), prewashed with Buffer A, was added and the mixture was rocked for another 30 min at 4°C. After centrifugation at 15,200 x g for 1 min, the supernatant was removed. Pelleted beads were washed 5 times with 0.5 mL Buffer A. Finally, 500 μL Buffer A was added to the beads and RNA and proteins were separated by phenol-chloroform-isoamyl alcohol extraction and precipitated as described previously (Rieder et al., 2012). From each coIP, 500-2000 ng of RNA was recovered. 100 μL of 1 × protein loading buffer [62.5 mM Tris-HCl, pH 6.8, 100 mM DTT, 10% (v/v) glycerol, 2% (w/v) SDS, 0.01% (w/v) bromophenol blue] was added to the final protein sample precipitated along with beads. This sample was termed the coIP sample. For verification of a successful coIP, protein samples equivalent to 1.0 OD_{600} of cells were obtained during different stages of the coIP (culture, lysate, supernatant, wash, and coIP (beads)) for further western blot analysis. One hundred microlitres of 1 × protein loading buffer was added to the protein samples and boiled for 8 min. Protein sample corresponding to an OD_{600} of 0.1 (culture, lysate, supernatant, and wash fraction) and 10 (for proteins precipitated from beads) were used for western blot analysis.

cDNA library preparation and deep sequencing

Residual gDNA was removed using DNase I treatment from the total RNA samples of the WT and mutant strains (see RNA isolation method below) or coIP RNA samples isolated from the control (WT) and Cas9-3xFLAG coIPs of *C. jejuni* NCTC11168 WT and *ΔcrRNA3* strains. cDNA libraries for Illumina sequencing were constructed by vertis Biotechnologie AG, Germany (http://www.vertis-biotech.com) in a strand-specific manner as described previously (Dugar et al., 2013). In brief, the RNA samples were poly(A)-tailed using poly(A) polymerase. Then, 5′-triphosphates were removed using tobacco acid pyrophosphatase (TAP), and an RNA adaptor was then ligated to the resulting 5′-monophosphate. First-strand cDNA was synthesized with an oligo(dT)-adaptor primer using M-MLV reverse transcriptase. In a PCR-based amplification step, using a high fidelity DNA polymerase, the cDNA concentration was increased to 10-20 ng/μL. For all libraries, the Agencourt AMPure XP kit (Beckman Coulter Genomics) was used to purify the DNA, which was subsequently analyzed by capillary electrophoresis.

A library-specific barcode for multiplex sequencing was included as part of a 3′-sequencing adaptor. The following adaptor sequences flank the cDNA inserts:

TruSeq_Sense_primer

5′-AATGATACGGCGACCACCGAGATCTACACTCTTTCCCTACACGACGCTCTTCCGATCT-3′

TruSeq_Antisense_NNNNNN_primer (NNNNNN = 6nt barcode for multiplexing)

5′-CAAGCAGAAGACGGCATACGAGAT-NNNNNN-GTGACTGGAGTTCAGACGTGTGCTCTTCCGATC(dT25)-3′

The samples were run on an Illumina HiSeq instrument with ~100 cycles in single-read mode. The resulting read numbers are listed in Table S1.

Analysis of RNA sequencing data

To assure high sequence quality, the Illumina reads in FASTQ format for both, RIP-seq and RNA-seq libraries, were trimmed with a cut-off phred score of 20 by the program fastq_quality_trimmer from FASTX toolkit version 0.0.13. After trimming, we applied the pipeline READemption (Förstner et al., 2014) version 0.4.3 for the following analysis steps: poly(A)-tail sequences were clipped from the 3′ ends of reads, size filtering was applied to eliminate read sequences shorter than 12 nt and the collections of remaining reads were mapped to the *C. jejuni* NCTC11168 (NCBI Acc.-No: NC_002163.1) genome using segemehl version 0.2.0 (Hoffmann et al., 2009) with an accuracy cut-off of 95%. Mapping statistics are listed in Table S1.

For the RIP-seq libraries, we used READemption (Förstner et al., 2014) to generate coverage plots representing the numbers of mapped reads per nucleotide. Reads that mapped to multiple locations contributed a fraction to the coverage value. For example, reads mapping to three positions contributed only 1/3 to the coverage values. Furthermore, the overlap of sequenced cDNA reads to annotations was assessed for each library via READemption (Förstner et al., 2014) by counting all reads overlapping selected annotations on the sense strand. These annotations consist of strain-specific NCBI gene annotations complemented with annotations of previously determined 5′ UTRs and small RNAs (Dugar et al., 2013). Each read with a minimum overlap of 10 nt was counted with a value based on the number of locations where the read was mapped. If the read overlapped more than one annotation, the value was divided by the number of regions and counted separately for each region (e.g., 1/3 for a read mapped to 3 locations).

For visualization in the Integrated Genome Browser (IGB) (Freese et al., 2016) and peak calling (see below), the coverage files of both coIPs were separately normalized via size factors calculated by applying the DESeq2 normalization (Love et al., 2014) to rRNA read counts of Cas9-3xFLAG and control library. This method was chosen as rRNA is unspecifically bound during coIP and hence should be equally present in the Cas9-3xFLAG and the control libraries.

For the RNA-seq libraries, we generated coverage files based on only the first nucleotide position of each read via READemption (Förstner et al., 2014). For visualization in the Integrated Genome Browser (IGB) (Freese et al., 2016), the coverage files were normalized to the number of reads that could be mapped from the respective library. To restore the original data range, each graph was then

multiplied by the minimum number of mapped reads calculated over all libraries. In addition, raw unnormalized coverage files were applied to detect endogenous Cas9 cleavage sites as described below.

Peak detection and binding motif analyses

In order to automatically define Cas9-bound RNA regions or peaks from the Cas9-3xFLAG coIP datasets, we applied an in-house tool "sliding_window_peak_calling_script" based on a sliding window approach that was originally developed to detect binding regions of CsrA in *C. jejuni* (Dugar et al., 2016). The script has been deposited at Zenodo (https://zenodo.org/record/49292) under DOI https://doi.org/10.5281/zenodo.49292 (https://doi.org/10.5281/zenodo.49292). The script is written in Python 3 and requires installation of the Python 3 packages *numpy* and *scipy* for execution.

In brief, the "sliding_window_peak_calling_script" software uses rRNA normalized wiggle files of the Cas9-3xFLAG and control coIP libraries as input to determine sites showing a continuous enrichment of the Cas9-3xFLAG-tagged library compared to the control. The identification of enriched regions is based on four parameters: a minimum required fold-change (FC) for the enrichment, a factor multiplied by the 90th percentile of the wiggle graph which reflects the minimum required expression (MRE) in the tagged library, a window size in nt (WS) for which the previous two values are calculated in a sliding window approach, and a nucleotide step size (SS) which defines the steps in which the window is moved along the genomic axis. All consecutive windows that fulfill the enrichment requirements are assembled into a single peak region. The peak detection is performed separately for the forward and reverse strand of each replicon. For the Cas9-3xFLAG coIP datasets, the following parameters were used: FC = 5, MRE = 3, WS = 25 and SS = 5.

Subsequently, we performed a manual curation of the 112 peaks predicted from the coIP in the wild-type strain by visual inspection of peak annotations together with cDNA coverage in the Integrated Genome Browser (IGB) (Freese et al., 2016). Based on the observed expression and enrichment patterns between Cas9-3xFLAG and control library, peaks were combined when likely representing a consecutive enriched site and split when possibly corresponding to multiple binding sites. The latter was only observed for the crRNAs and tracrRNA, for which individual peak regions were then defined based on their annotation. Furthermore, a refinement of peak boundaries was conducted and the resulting 96 peaks were checked for their presence in the Δ*crRNA3* coIP.

For the prediction of consensus motifs based on the peak sequences, MEME (Bailey and Elkan, 1994) was used.

crRNA base-pairing predictions

The NUPACK (http://www.nupack.org/) analysis tool was used to predict every possible binding permutation between the processed spacer sequences and the enriched and curated RNA sequences. The settings were set as follows: RNA species, 37°C, 2 strand species, 2 maximum complex size, and each species was set to an arbitrary concentration of 1 μM. The predicted equilibrium concentrations of strand 1 (processed spacer), strand 2 (enriched RNA sequence), and strand1-strand2 were then recorded. To calculate the equilibrium binding constants, the equilibrium concentration of strand1-strand2 was divided by the product of the equilibrium concentrations for strand1 and strand2.

Cas9 cleavage-site analysis

Automated detection of Cas9 cleavage sites within annotated peak regions was conducted by extracting coverage values of WT and Δ*cas9* libraries for each nt position covered by a peak. Afterwards, differential cDNA count expression between WT and Δ*cas9* library was determined for each annotation using GFOLD version 1.1.4 (Feng et al., 2012) but with manually-defined normalization constants based on the number of reads that could be mapped to the respective library. All positions with a GFOLD (0.01) value > 0 were considered and, in case multiple such positions existed for a single peak, the position with the highest GFOLD (0.01) was annotated as the potential cleavage site.

Base-pairing and cleavage-site comparison

To determine the location of each cleavage site relative to the predicted crRNA binding site, we selected the predicted binding site closest to the cleavage site. For the longest enriched RNA peak (1,080 nts) within Cj0358 mRNA, we repeated the base-pairing predictions with each crRNA and 100 nts upstream and downstream of the cleavage site. In all but one case, the crRNA bound to this site also had the highest binding affinity compared to the other crRNAs. Once a binding site was selected for each cleaved RNA peak, we identified the closest base pair to the cleavage site. We then counted the number of nucleotides between this base-paired nucleotide in the RNA peak and the cleavage site. The location of the base pair within the crRNA served as a reference to compute the location of the cleavage site relative to the 5′ end of the crRNA. Predicted crRNA binding sites and distances to the cleavage site are reported in Table S2.

SDS-PAGE and immunoblotting

Protein analyses were performed on cells collected from *C. jejuni* in mid-exponential phase (OD_{600} 0.5-0.6) or *E. coli* cultures in late-exponential phase (OD_{600} 1.0-1.5). Cells were collected by centrifugation at 11,000 x g for 3 min. Cell pellets were resuspended in 100 μL of 1 × protein loading buffer [62.5 mM Tris-HCl pH 6.8, 100 mM DTT, 10% (v/v) glycerol, 2% (w/v) SDS, 0.01% (w/v) bromophenol blue] and boiled for 8 min. For western blot analysis, samples corresponding to an OD_{600} of 0.1 were separated by 12% (v/v) SDS-PAA gels and transferred to a nitrocellulose membrane by semidry blotting. Membranes were blocked for 1 h with 10% (w/v)

milk powder/TBS-T (Tris-buffered saline-Tween-20) and incubated overnight with primary antibody at 4°C. Membranes were then washed with TBS-T, followed by 1 h incubation with secondary antibody. After washing, the blot was developed using enhanced chemiluminescence (ECL)-reagent. Cas9-3xFLAG was detected with monoclonal anti-FLAG primary antibody (1:1000 in 3% BSA/TBS-T; Sigma-Aldrich, #F1804-1MG, RRID: AB_262044) and anti-mouse IgG secondary antibody (1:10,000 in 3% BSA/TBS-T; GE-Healthcare, #RPN4201). Untagged WT and mutant forms of Cas9 were detected using anti-Cas9 serum (1:1000 in 3% BSA/TBS-T) (Louwen et al., 2013) and an anti-rabbit IgG secondary antibody (1:10,000 in 3% BSA/TBS-T; GE-Healthcare, #RPN4301, RRID:AB_2650489). A monoclonal antibody specific for GroEL (1:10,000 in 3% BSA/TBS-T; Sigma-Aldrich, # G6532-5ML, RRID:AB_259939) and an anti-rabbit secondary antibody were used as a loading control.

RNA isolation

C. jejuni strains were grown to mid-exponential growth phase (OD_{600} ~0.6) in Brucella broth and culture volume corresponding to a total amount of 4 OD_{600} was harvested and mixed with 0.2 volumes of stop-mix (95% ethanol and 5% phenol, vol/vol). The samples were snap-frozen in liquid nitrogen and stored at −80°C until RNA extraction. Frozen samples were thawed on ice and centrifuged at 4°C to collect cell pellets. Cell pellets were lysed by resuspension in 600 μL of a solution containing 0.5 mg/ml lysozyme in TE buffer (pH 8.0) and 60 μl 10% SDS. The samples were incubated for 1–2 minutes at 65°C to ensure lysis. Afterwards, total RNA was extracted using the hot-phenol method as described previously (Dugar et al., 2013).

Northern blot analysis

For Northern Blot analysis, 5 to 10 μg RNA sample was loaded per lane. After separation on 6% polyacrylamide (PAA) gels containing 7 M urea, RNA was transferred to Hybond-XL membranes (GE-Healthcare) by electroblotting. After blotting, the RNA was UV cross-linked to the membrane and hybridized with γ32P-ATP end-labeled DNA oligonucleotides (Table S3).

In-vitro T7 transcription and RNA labeling

DNA templates containing the T7 promoter sequence were generated by PCR using oligos and DNA templates listed in Table S3. The DNA template for crRNA3 was prepared without amplification by directly hybridizing CSO-2191 and CSO-2192. T7 *in-vitro* transcription of RNAs was carried out using the MEGAscript T7 kit (Ambion) and sequences of the resulting T7 transcripts are listed in Table S3. *In-vitro* transcribed RNAs were quality checked and 5′ end-labeled (γ^{32}P) as previously described (Dugar et al., 2016).

PAM-SCANR analysis of CjCas9

The previously described PAM-SCANR method was used to analyze the recognized PAMs for *C. jejuni* Cas9 (Leenay et al., 2016). In short, Campy_dCas9_pBad33_J23108 was combined with a PAM-SCANR targeting sgRNA and a five nucleotide 5′-CCNNNNNC-3′ library spanning what was originally considered a 5′-NNNNACA-3′ PAM - where the N's correspond to the unrecognized linker region of the PAM. After GFP-based selection for recognized PAMs was performed, recognized PAMs were identified through sequencing of the GFP-positive cells. PAMs were extracted from the sequencing reads and plotted using the Krona software package (https://github.com/marbl/Krona/wiki) (Ondov et al., 2011).

After the PAM-SCANR sequencing data was analyzed, another manuscript was published that identified PAMs recognized by the *C. jejuni* Cas9 using an *in vitro* cleavage assay (Kim et al., 2017). Their sequencing data was downloaded and a PAM wheel was created from their sequencing data. This data highlighted the fact that the 8th nucleotide (set as a constant "C" in the PAM-SCANR method) actually is recognized by the Cas9.

E. coli plasmid clearance assay

All plasmid clearance assays were based on a previously published method (Gomaa et al., 2014). *E. coli* cells containing both the Cas9 and targeted plasmid were grown up in selective media, prepared to be electrocompetent, and transformed with 50 ng of targeting sgRNA plasmid in biological triplicates. Experiments using Cas9 plasmids with an sgRNA in the backbone were performed by growing up *E. coli* strains containing the targeted plasmid and then transforming in 50 ng of the Cas9+sgRNA plasmid. All spacers tested were compared directly to a non-targeting sgRNA control. All plated cells were diluted to observe a countable CFUs after non-selective recovery in SOC medium. To calculate the fold-reduction in transformation efficiency, the non-targeting CFUs were divided by the CFUs after targeting by *C. jejuni* Cas9.

After transformation, cells were directly plated on selective solid media unless otherwise noted. To perform the additional outgrowth required to observe plasmid clearance for the WT Cas9 and a weakly recognized ACAD (D = Not C) PAM, an additional partially selective outgrowth was used. After the 1 hour non-selective liquid recovery in SOC, the recovered cells were diluted 1:1,000 into LB media for 16 hours with antibiotics selecting only for plasmids that were present prior to the electroporation. After this additional outgrowth, the recovered cells were again diluted prior to plating on fully selective solid media. All biological replicates were outgrowths from the same samples subjected to fully selective solid media after the original, non-selective SOC recovery.

Primer extension

Ten micrograms of DNase I-digested RNA, extracted from the exponential phase of *C. jejuni* NCTC11168 strains, was concentrated in 5.5 μL water. 1μL of γ32P-ATP end-labeled oligodeoxyribonucleotide probe CSO-2110 were mixed with the RNA samples and

incubated at 80°C. The temperature was gradually shifted to 42°C over a period of 1 hr. Each of the samples was then mixed with 1 μL 10 mM dNTPs, 2 μL 5x AMV RT buffer and 0.5 μL AMV RT 20 u/μL (Fermentas, #EP0641) and incubated further at 42°C for 1 hr. Samples were denatured for 3 min at 95°C and half of the reaction was separated on a 6% polyacrylamide/8.3 M urea sequencing gel in 1X TBE. Sequencing ladders were generated according to the manufacturer's instructions by SequiTherm EXCEL II DNA Sequencing Kit (Epicenter Biotechnologies) using the same primers and PCR-amplified Cj1321 locus from NCTC11168 (Oligos CSO-1248 and CSO-0837) as template. 2 μL of the sequencing reactions were loaded on the same gel as reference.

In-vitro DNA cleavage assay

For the verification of the PAM-sequence and PAM-dependent DNA cleavage by Cas9 *in vitro*, oligos were 5′ end-labeled (γ^{32}P) and duplexes were formed by slowly cooling (2 min at 75°C, then 10 min in 10°C steps from 65 - 25°C) the two complementary strands at a final concentration of 50 nM (CSO-3728 + CSO-3729 for *cj1321* + PAM, CSO-3730 + CSO-3731 for WT *cj1321*, CSO-3708 + CSO-3709 for ACAC PAM, CSO-3723 + CSO-3722 for TGTG PAM control). The sgRNA scaffold was designed according to previously predicted sgRNA for *Campylobacter lari* (Ran et al., 2015). The T7 *in vitro* transcribed cr3, NC, and CC sgRNAs were folded in a 3μM stock solution (2 min 95°C, then 10 min in 10°C steps from 75 - 25°C). Cas9-sgRNA complexes were formed with 1.5 μL 3 μM Cas9 and 1.5 μL 3 μM sgRNA in 13.8 μL reaction volume including 3 μL 5x reaction buffer (750 mM KCl, 100 mM HEPES [pH 7.5], 5% glycerol, 25 mM MgCl2, and 5 mM DTT) for 10 min at room temperature. Next, 1.2 μL of 50 nM oligo dimers were added and incubated at 37°C for 5 min (O'Connell et al., 2014). The final reaction contained 300 nM of Cas9-sgRNA complex and 4 nM of the target DNA. Similar reactions with water instead of Cas9 were used as control. The reactions were stopped by addition of one volume of loading buffer II (#AM8546G, Ambion) and samples were stored at −20°C until they were analyzed on a 8% PAA / 7M urea sequencing gel in 1x TBE buffer. Before running, samples were denatured at 95°C for 5 min. Gels were dried, exposed to a screen, and analyzed using a PhosphorImager (FLA-3000 Series, Fuji).

In-vitro RNA cleavage assays

For the investigation of Cj1321 mRNA cleavage and programmable RNA cleavage, target T7 RNAs (Cj1321 or *flaA*) were 5′ end-labeled (γ^{32}P). Unlabeled cr3, NC, CC, fla1, fla2, and fla3 sgRNAs were designed and folded as described above. Cas9-sgRNA complexes were formed with 1.5 μL 10 μM Cas9 and 1.5 μL 10 μM gRNA in 13.5 μL reaction volume including 3 μL 5x reaction buffer (750 mM KCl, 100 mM HEPES [pH 7.5], 5% glycerol, 25 mM MgCl2, and 5 mM DTT) (O'Connell et al., 2014) and 1.5 μL yeast tRNAs (1 mg/mL, Ambion AM7119) for 10 min at room temperature. 1.5 μL of labeled target RNA was then added to a final concentration of 4 nM and cleaved at 37°C for 5 or 60 min. The final reaction contained 1 μM Cas9 in complex with equal concentration of sgRNA, crRNA or tracrRNA and 4 nM of the target RNA. For RNase T1 ladders, ∼0.2 pmol labeled RNA was denatured in 1x Structure Buffer (Ambion 9751G) for 1 min at 95°C, cooled to 37°C and incubated with 0.1 U RNase T1 for 5 min at 37°C. The OH ladder was generated by incubation of ∼0.2 pmol labeled RNA in 1x alkaline hydrolysis buffer (Ambion, 9750G) for 5 min at 95°C. All reactions were stopped with one volume of loading buffer II and analyzed in the same manner as described above. The specific reaction conditions were selected based on prior RNA and ssDNA cleavage assays performed with Cas9 cited above.

QUANTIFICATION AND STATISTICAL ANALYSIS

For the PAM analysis in *E. coli*, biological replicates were performed on unique single colonies, and error was calculated with standard deviation, or SEM (Standard deviation/sqrt[n]) as defined in the figure legend.

DATA AND SOFTWARE AVAILABILITY

The raw, de-multiplexed reads and unnormalized coverage files of the RIP- and RNA-seq libraries representing whole read coverage, the raw PAM-SCANR fastq reads, and the calculated PAM enrichments have been deposited in the NCBI Gene Expression Omnibus (Edgar et al., 2002) under the accession number GSE106849.

The 'sliding_window_peak_calling_script' for identification of Cas9-binding sites based on RIP-seq data has been deposited at Zenodo (https://zenodo.org/record/49292) and is available via DOI under https://doi.org/10.5281/zenodo.49292. The unprocessed and uncompressed gel images have been published at Mendeley under https://doi.org/10.17632/r9sc7f3ybv.1.